The RESEARCH LABORATORY

of

ELECTRONICS

at the

MASSACHUSETTS INSTITUTE OF TECHNOLOGY
CAMBRIDGE, MASSACHUSETTS 02139

A Touch Lab Report

Experimental Determination of the Viscoelastic

Properties of the Human Fingerpad
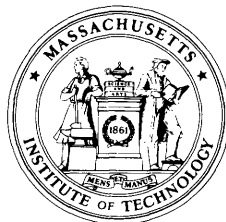
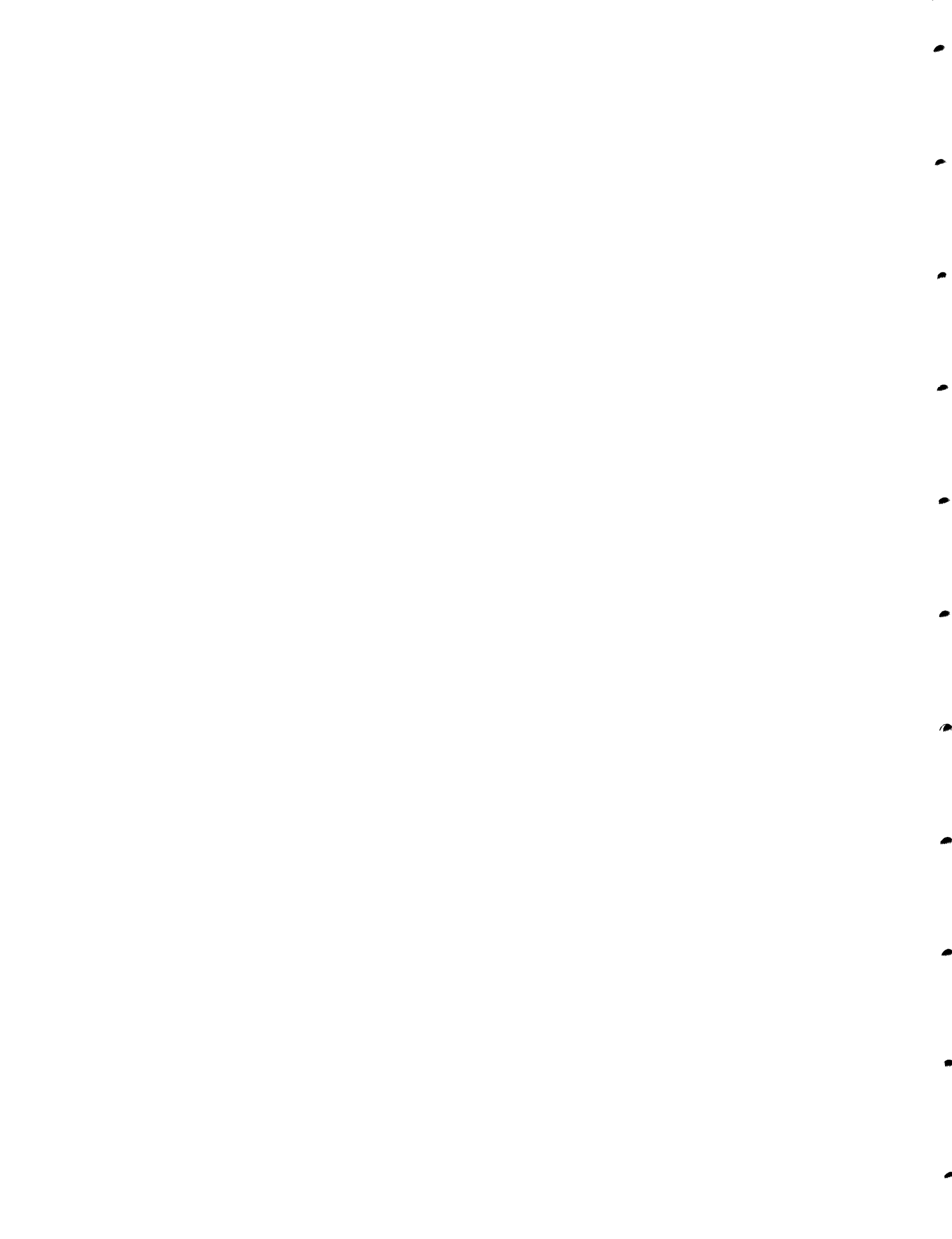Amanda Sue Birch and Mandayam A. Srinivasan

A Touch Lab Report

Experimental Determination of the Viscoelastic Properties of the Human Fingerpad

Amanda Sue Birch and Mandayam A. Srinivasan

RLE Technical Report No. 632

September 1999

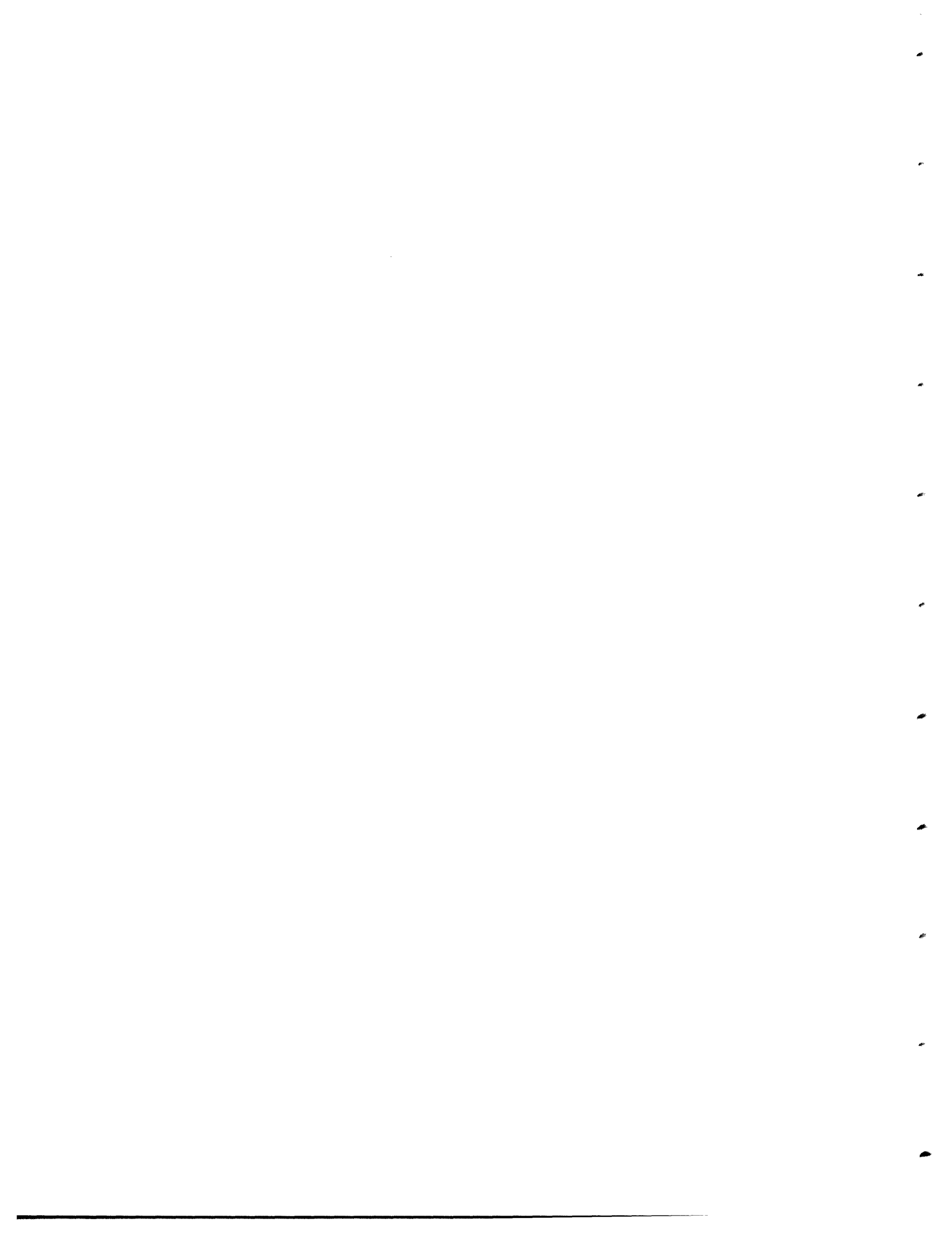# Experimental Determination of the Viscoelastic Properties of the Human Fingerpad

by

Amanda Sue Birch

Massachusetts Institute of Technology
Submitted to the Department of Mechanical Engineering
on May 9, 1998 in partial fulfillment of the
requirements for the Degree of Master of Science in
Mechanical Engineering

ABSTRACT

Understanding the human tactile system is the motivation for this research. The linear viscoelastic mechanical properties of the human fingerpad describe the stress-strain relationship within the fingerpad for any stimulus geometry and any time history of applied forces or displacements. The stress-strain relationships within the fingerpad tissue govern the stimuli to the mechanoreceptors which are the source of all tactile information to the brain.

A device referred to as the tactile stimulator was designed and is presented in this work. The tactile stimulator is a versatile device that can provide a variety of dynamic stimuli to any material and measure the displacement and force responses. The stimuli can vary with time and with indentor shape. The device is currently configured to allow normal or tangential displacement-controlled stimuli. The tactile stimulator has a force resolution of less than 1 mN and a displacement resolution of less than 1 μm.

The solution to the linear elastic problem of a cylindrical punch indenting a semi-infinite half-space can be transformed to a linear viscoelastic solution by means of the correspondence principle. Two of a material functions can completely describe any force-displacement or stress-strain relationship within the material. To determine the mechanical properties of the human fingerpad *in vivo*, two linearly independent experiments in the linear range of the tissue were performed to solve for the dynamic, viscoelastic mechanical properties of the human fingerpad. The impulse response bulk modulus and the impulse response shear modulus are defined in this thesis as a function of frequency. The impulse response bulk modulus varies from 55 kPa at 2 Hz to 8 MPa at 200 Hz. The impulse response shear modulus varies from 90 kPa at 2 Hz to 8 MPa at 100 Hz.

Thesis Supervisor: Mandayam A. Srinivasan
Title: Principal Research Scientist

TABLE OF CONTENTS

LIST OF TABLES

LIST OF SYMBOLS

θ .... *Armature Angle*
Ω .... *Ohms*
μm .... *Micrometer*
δ_x .... *Tangential Displacement*
δ_z .... *Normal Displacement*
A .... *Ampere*
a .... *Radius of Cylindrical Punch*
A/D .... *Analog to Digital*
AC .... *Alternating Current*
$AMELIA$ .... *Application Module Link Interface Adapter*
B .... *Viscous-Friction Coefficient*
CPU .... *Central Processing Unit*
D/A .... *Digital to Analog*
dB .... *Decibel*
DC .... *Direct Current*
DOS .... *Disk Operating System*
$DPRAM$ .... *Dual Port Random Access Memory*
DSP .... *Digital Signal Processor*
e_a .... *Motor Input Voltage*
e_b .... *Back emf Voltage*
emf .... *Electromotive Force*
$EPROM$ .... *Executable Programable Read Only Memory*
F_x .... *Tangential Force*
F_z .... *Normal Force*
G .... *Shear Modulus*
Hz .... *Hertz*
I/O .... *Input/Output*
i_a .... *Armature Input Current*
J .... *Moment of Interia*
K .... *Amplifier Gain, Bulk Modulus, or MotorTorque Constant*
$k\Omega$ .... *Kiloohms*
K_{cr} .... *Critical Gain*
kg .... *Kilogram*
kHz .... *Kilohertz*
K_p .... *Proportonal Controller Term*
kPa .... *Kilopascal*
L_a .... *Armature Inductance*
LCD .... *Liquid Crystal Display*
m .... *Meter*

CHAPTER 1

INTRODUCTION

1.1 Introduction to Haptics

Haptics is a relatively new field of study in the realm of sensory communications. In general, haptic research involves all aspects of human hands and their interactions with objects, including mechanics, dynamics, sensorimotor functions, and cognition. Biomechanics, neurophysiology, and psychophysics all assume important roles in the field of haptics. Hapticians usually come from a variety of backgrounds, including mechanical engineering, brain and cognitive sciences, electrical engineering, computer science, and medicine.

With such a diverse group of people involved in the field, several end goals of haptics exist. The three main categories of goals for haptic research include robotics, medical applications, and human-machine interfaces for virtual environments and teleoperation.

Robotic applications are commonly related to industry. For example, a robot needs to "sense" how tight its grip on an object is; the robot should neither crush nor drop and object because both actions could result in damage. Haptic research deciphers how the

human tactile sensing and motor processes contribute to the performance of this specific task The algorithm may then be useful for programming a robot.

Similarly, threshold algorithms can also be applied in the world of medicine. Prosthetic hands might be programmed in a manner analogous to the previously mentioned robot. Within the field of medicine, virtual surgery is another example of a revolutionary technology pursued by hapticians. Understanding how humans sense the pressure of a scalpel's cutting action and developing a computer program to simulate surgery will revolutionize medical training.

Virtual environments are also being developed as applications of haptics. Virtual video games allow the user to actually feel objects. More complex virtual environments, such as flight simulation programs, are being developed to enhance military training. Teleoperations, including flying aircraft from a remote position, will eventually render the most dangerous missions obsolete. Haptics reveals important considerations for designing many other types of tactile displays and human-machine interfaces as well. With such a broad range of applications for the study of haptics, the list of possible goals is virtually infinite.

1.2 Mechanics of Touch

This thesis is focused specifically on the biomechanics of touch at the human fingerpad level. It is important to understand the mechanistic phenomena that occur when a human touches an object. When a person touches an object, the tactile information sent to the brain is based upon the spatio-temporal distribution of mechanical loads on the fingerpad (Phillips and Johnson 1981, Srinivasan and Dandekar 1996). These mechanical loads create a stress-strain field that is sampled by specialized nerve terminals within the skin known as mechanoreceptors. The mechanoreceptors then encode this information as neural impulses which are sent to the brain. There are three basic questions that need to be addressed concerning tactile sensing: 1) What is the contact mechanics between the object and the fingerpad? 2) How are the mechanical loads transmitted through the skin? and 3) How do mechanoreceptors transform these signals into neural impulses? This

research seeks to answer a part of the second question by defining the material properties of the fingerpad.

The specific area of the finger to be characterized is located on the palm side of the distal phalanx. This area is typified by finger ridges that characterize the human fingerprint. Fingertips are normally used for tactile exploration; therefore they are a logical area to study in detail. In addition to being the area most commonly used for tactile exploration, this area also contains the highest density of mechanoreceptive cells in the whole human body with approximately 250 receptors per cm^2 (Vallbo and Johansson 1984).

The mechanoreceptors are made up of four different types of cells. Of the 250 receptors per cm^2, approximately 60% are Meissner's corpuscles, also know as rapidly adapting (RA) mechanoreceptors; 30% are Merkel's cells, also known as slowly adapting type I (SAI); 5% are Pacinian corpuscles (PC); and the remaining 5% are Ruffini's corpuscles (SAII) (Kandel and Jessell 1991). The RA units and the PC units usually respond to skin indentation when the stimulus is in motion. The SAI and SAII units are sensitive to both static and moving stimuli (Johansson, Landström, and Lundström 1982, Kandel and Jessell 1991).

In order to stimulate these mechanoreceptors, a load must be applied to the skin. The load can be specified as a force or a displacement. These loads translate to a stress-strain field throughout the fingerpad. Phillips and Johnson (1981), as well as Srinivasan and Dandekar (1996), have shown that the neural encoding at the mechanoreceptor depends upon the stress-strain field at the mechanoreceptor. In order to determine the stress-strain state of the tissue at a mechanoreceptor, one must first understand how the fingerpad tissue behaves in response to a stimulus. Determining the material properties of the fingerpad is an essential step in understanding the stress-strain fields created within the fingerpad tissue when a human touches an object.

1.3 Previous Research

Investigating the mechanical properties of human skin is not a new concept; however, the goals of previous investigations varied greatly and few studies focused on the *in vivo* biomechanical properties of the human tactile system.

Several studies were performed from a haptic viewpoint with the goal of better understanding the neurophysiological and psychophysiological aspects of the sense of touch. Bolanowski *et al.* (1988) and Vallbo and Johansson (1984) applied vibrational indentation stimuli on the human fingerpad, but focused on the psychophysiological and neurophysiological phenomena. Rabinowitz *et al.* (1987) also applied vibrational indentation stimuli to the human fingerpad, varying vibration intensity, frequency, and contactor area. The resulting tuning curves are useful for understanding the psychophysics of touch, but do not provide insight on the biomechanics of the fingerpad.

From a biomechanics viewpoint, several studies have addressed the determination of the mechanical properties of skin. Von Gierke *et al.* (1952) applied vibrations from 10 Hz to 2000 Hz to the thigh and upper arm to understand how energy is absorbed by the body via mechanical impedance. Lanir (1987) gave a complete description of the function of skin, including some mechanical properties that are useful to the application of plastic surgery, in particular stretch. Many studies were also performed *in vitro* to better understand the mechanical properties of the skin. These studies do give us some insight as to what we might expect to find *in vivo*; however, living tissues are more complex and exhibit different properties.

This research limits the investigation of the mechanical properties of human skin to the fingerpad, the most common source of tactile stimulation. The living tissue of the fingerpad has distinctive characteristics. It is important, therefore, to focus specifically on the fingertip *in vivo* if we wish to decode the tactile information sent to the brain.

Several *in vivo* studies have been conducted with a goal of determining the mechanical properties of the human fingerpad. Based on fingertip surface displacement under a line load, Srinivasan (1989) developed a "water-bed" model of the fingerpad. This research modeled the fingerpad as an elastic membrane filled with an incompressible fluid under plane strain conditions. Two and three dimensional homogeneous and layered models of the fingerpad were then developed incorporating a linear elastic material property and realistic fingerpad external geometry (Dandekar and Srinivasan 1995, Srinivasan and Dandekar 1996).

Gulati and Srinivasan (1995, 1997) applied sinusoidal displacements to the fingerpad and measured resulting forces. The study was limited to frequency inputs in the range of 0.125 Hz to 16 Hz and most data collected were at an indentation depth that gave a nonlinear force-displacement relationship. These authors also varied indentor shapes. Srinivasan *et al.* (1998) used this data to develop a lumped parameter model of the fingerpad tissue. De and Srinivasan (1998) computed one material function of the fingerpad tissue using normal force-displacement relationships. Two independent material functions could not be computed due to a lack of data.

Pawluk and Howe (1996a,b) performed sinusoidal experiments over a larger range of frequencies (0.5 Hz to 1024 Hz) and developed a model for both lumped and distributed responses. These authors modeled a bulk response of the fingerpad and associated this mechanical response with the response of the mechanoreceptors. The experiments involved contact nonlinearities and assumed that the fingerpad tissue is incompressible. This model showed that the force-displacement response of the fingerpad tissue is dependent upon the size of the subject's fingerpad.

Serina *et al.* (1997) also modeled a bulk response of the fingerpad over the range of frequencies from 0.25 Hz to 3 Hz. This is a range of frequencies commonly associated with occupational injuries resulting from repetitive tasks such as typing. The model developed involved contact nonlinearities because a subject is tapping a flat plate. This

15

work showed the stiffness of the fingerpad, at various contact angles with the plate, over a limited range of frequencies.

All of these studies provide a sound foundation and validation source for this research. This work is an extension of the research conducted by De and Srinivasan (1998). Two independent material functions will completely describe the three-dimensional, linear, viscoelastic behavior of the *in vivo* human fingerpad tissue.

1.4 Motivation

The biomechanics of the human fingerpad must be understood before we can reach the goals of smart industrial robots, prostheses with a sense of touch, and virtual simulators. Characterizing material properties of the fingertip *in vivo* is an essential first step toward a better understanding of the human tactual system. Providing an accurate model of linear deformations of the human fingerpad during tactile exploration is a critical step in the process of decoding tactile stimuli. This work seeks to provide a quantitative, physically based model of the mechanical behavior of the human fingertip tissue in the linear range.

This work focuses on finding the material functions of the fingerpad. Determining the material properties of the human fingerpad tissues, as opposed to developing a model based on the geometric configuration of the fingerpad, provides the foundation necessary to develop more complex models. Once the material properties are known, issues such as contact nonlinearities and variant fingerpad shapes can be incorporated in a straight-forward manner. This approach allows the stress-strain relationship to be determined anywhere in the fingerpad, a key to decoding neural responses to tactile stimulation.

Some frequency response data were collected previously, but only in the range of 0 Hz to 32 Hz, as compared to the 2 Hz to 200 Hz range of this research. Furthermore, in most of the previous experiments, no intentional measures were taken to avoid nonlinear effects such as dynamic contact mechanics, large deformations, and material nonlinearities. This research takes special care to ensure linearity in three main areas; effects of contact nonlinearities, geometric nonlinearities, and material nonlinearities are minimized in these

experiments. The approach is to understand first the mechanics in the linear range before trying to develop a more complicated, nonlinear model. This approach will allow us to develop simple but efficient dynamic, linear material models.

In addition to the importance of the material functions obtained in this research, the hardware developed for this project has important implications in better understanding the sense of touch. First, the tactile stimulator operates at a high precision level with less than 1 μm resolution for position and less than 1 mN resolution for force. This precision allows data collection in the narrow linear domain of the tissue. Furthermore, the machine is designed to be used for different types of experiments—various input signals, control algorithms, or stimulus shapes. This tactile stimulator could be used for perceptual experiments as well.

1.5 Overview of Thesis

Before the specifics of this project are explored, theory concerning the model of the fingerpad is explained. This theory drives the decisions made in the three fundamental phases of this project. To obtain the linear viscoelastic material functions of the human fingerpad, the three phases of research are: 1) a construction phase, 2) an experimental phase, and 3) a data analysis and conclusions phase.

The construction phase involved building the high precision, one degree of freedom tactile stimulator for use in the experimental phase. This device can provide a variety of indentation stimuli to the human fingerpad. Stimuli are generally displacement controlled, and the device is capable of providing step, ramp, sinusoidal, square wave, or noise stimuli to the fingerpad. The tactile stimulator can be configured to provide normal or shear indentations to the skin. A variety of probe shapes can be attached as well. The flexibility of the tactile stimulator makes it a valuable device.

During the experimentation, the tactile stimulator was used to collect force-displacement data from the fingerpad tissue. Force response data were collected for sinusoidal displacement stimuli applied both normally and tangentially to the resting fingerpad. The

frequencies of the applied vibrations were in the range of 2 Hz to 200 Hz. Five subjects were used for all experiments to date.

After data collection, determination of the material functions commences. Bode plots were generated to provide a profile of the frequency response of the fingerpad for both shear and normal stimuli. Using the two linearly independent experiments and two separate equations—normal and shear force-displacement relationships—with two unknowns, the impulse response shear modulus and the impulse response bulk modulus are found. These frequency dependent material functions completely describe the three-dimensional, linear viscoelastic behavior of the human fingerpad tissue.

CHAPTER 2

THEORY

The living tissue of the human fingerpad is complex. The fingerpad tissue is most likely viscoelastic, nonlinear, anisotropic, and inhomogeneous (Lanir 1987). A model capturing all of these features would be complex and perhaps even unnecessary for the desired applications. Despite the complexity of the fingerpad material, several assumptions lead to a relatively simple model that captures the salient mechanical properties.

Based on experimental evidence, De and Srinivasan (1998) assert three reasons why the human fingerpad should be modeled as a viscoelastic material. First, the force response is clearly strain rate dependent. When the fingerpad is stimulated with ramp-and-hold displacements, the steady state force response is only a function of the depth of indentation; however, the transient response is dependent on the ramp velocity. Secondly, previous experimental data show stress relaxation, evidenced by a decrease from a peak force value at the end of a displacement ramp to a steady state value. Finally, the presence of hysteresis indicates that energy is being dissipated. These three characteristics observed in previous data provide a solid basis for assuming the human fingerpad tissue is a viscoelastic material.

Specifically, the fingerpad tissue is modeled as a linear viscoelastic material in this work. Previous research (Srinivasan *et al.* 1998) shows that the force-displacement curves can be linearized within a certain range of the origin. Several experiments are performed in this work specifically to ascertain that the experiments are conducted within the linear range of the tissue. This verification will be discussed further in Section 5.1.

Two final assumptions are made to simplify the model. The material is assumed to be homogenous and isotropic. These assumptions allow this research to concentrate on the rate-dependent behavior of the tissue in the linear regime.

The overall objective is the determination of the linear viscoelastic material functions of the human fingerpad. The linear elastic solution for a cylindrical punch indenting a semi-infinite half space is used to find the viscoelastic solution using the correspondence principle (De and Srinivasan 1998). Two independent material functions are expressed as a function of frequency. These two properties completely describe the behavior of the material, based on the assumptions stated above.

Any linear isotropic viscoelastic material is completely described by any two independent material functions. The two material functions defined in this research are the impulse response bulk modulus $\overline{K}(s)$ and the impulse response shear modulus $\overline{G}(s)$. Any of the other common material functions, such as Young's modulus or Poisson's ratio, can be written in terms of the bulk modulus and the shear modulus. Two properties must be determined to characterize the material; therefore it is necessary to develop two linearly independent experiments to uniquely determine the two material functions (De 1998). In this case, it is convenient to perform experiments with controlled displacements in both the normal and tangential directions. This results in two linearly independent equations with two unknown material functions.

The underlying elastic solution is a well known solution for a cylindrical punch indenting a semi-infinite half space. The derivation is given by Johnson (1985). For a sufficiently small radius of the indenting punch, the semi-infinite half space assumption holds. The

20

solution also assumes that no global sliding occurs. Since the fingerpad is glued to the indentor, no global sliding occurs in these experiments. Finally, this solution does not include dynamic contact mechanics. The area of contact between the fingerpad and the indentor remains constant at all times.

The theory below is developed in parallel for the experiments in the normal and the tangential directions. Equations for the normal experiments are on the left and are annotated with (a). Equations for the tangential experiments are on the right and are annotated with (b). Figure 2.1 schematically shows the nature of the problem and defines the basic terms used in the following derivation. The variables F_z and F_x refer to the normal and tangential forces respectively while δ_z and δ_x refer to the normal and tangential displacements.
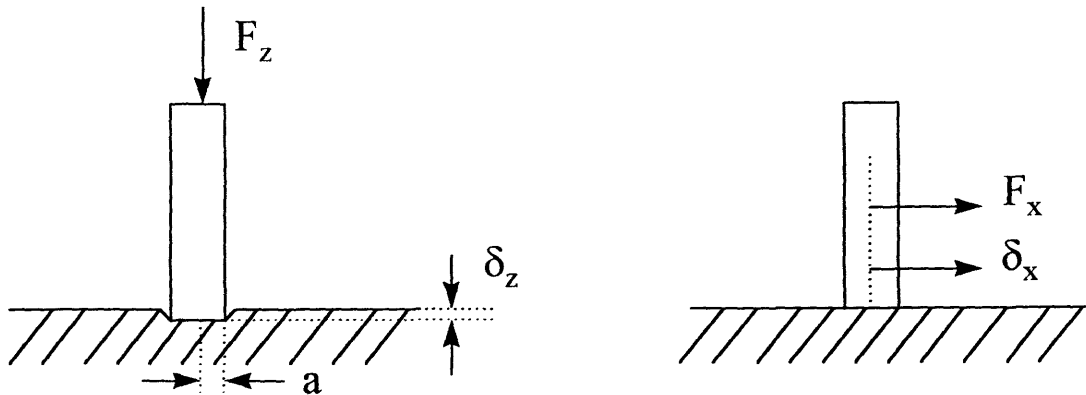
Figure 2.1: Cylindrical Punch Indenting a Semi-Infinite Half Space in normal (left) and tangential (right) directions

Equation 2.1 (a) and Equation 2.1 (b) quantify the force-displacement relationships shown in Figure 2.1 (Johnson 1985). These equations represent the force-displacement relationships for a cylindrical punch indenting a linear, elastic, isotropic, homogenous medium where the semi-infinite half-space assumption is valid. The symbol a represents the radius of the cylindrical punch, G is the elastic shear modulus, and K is the elastic bulk modulus.

$$\frac{F_z}{\delta_z} = \frac{8aG(3K+G)}{3K+4G} \qquad\qquad \frac{F_x}{\delta_x} = \frac{16aG(3K+G)}{3(3K+2G)}$$

Equation 2.1 (a)   Equation 2.1 (b)

Equation 2.1 (a) and Equation 2.1 (b) represent purely elastic solutions to the problem at hand. These equations, developed for purely linear elastic problems, may be extended to represent the behavior of viscoelastic materials under quasi-static loading using the correspondence principle (Lee 1955). The method of transforming the elastic solution to the viscoelastic solution is shown by De and Srinivasan (1998). The relationship between the linear elastic solution and the linear viscoelastic solution is reiterated here because the implications are critical to understanding the data presented in this work.

In the time domain, Hooke's law takes the form presented in Equation 2.2 for three-dimensional linear viscoelasticity. In these equations, $S_{ij}(t)$ and $\sigma_{kk}(t)$ represent the deviatoric and volumetric components of the Cauchy stress tensor, respectively. The symbols $e_{ij}(t)$ and $\varepsilon_{kk}(t)$ represent the deviatoric and dilatational strain tensor components. Time is represented by t. The material functions are $G(t)$, the linear viscoelastic shear modulus, and $K(t)$, the linear viscoelastic rigidity modulus.

$$\sigma_{kk}(t) = 3\overline{K}(t) * \varepsilon_{kk}(t) \qquad\qquad S_{ij}(t) = 2\overline{G}(t) * e_{ij}(t)$$
$$\{i,j,k\} \in [1,3]$$

Equation 2.2

The convolution operator in Equation 2.2 is defined by Equation 2.3.

$$f(t) * g(t) = \int_{0^-}^{t} f(t-\tau)g(\tau)d\tau$$

Equation 2.3

In the frequency domain, Hooke's law takes the form presented in Equation 2.4. $\bar{S}_{ij}(s)$ and $\bar{\sigma}_{kk}(s)$ represent the Laplace transforms of the deviatoric and volumetric components of the Cauchy stress tensor, respectively. Similarly, $\bar{e}_{ij}(s)$ and $\bar{\epsilon}_{kk}(s)$ represent the Laplace transforms of the deviatoric and dilatational strain. The two material functions are represented by $\bar{G}(s)$, the impulse response rigidity modulus, and $\bar{K}(s)$, the impulse response bulk modulus. The symbol s represents the Laplace transform variable, which is frequency in radians per second. The impulse response material functions therefore define the relationship between the stresses and the strains.

$$\bar{\sigma}_{kk}(s) = 3\bar{K}(s)\bar{\epsilon}_{kk}(s) \qquad\qquad \bar{S}_{ij}(s) = 2\bar{G}(s)\bar{e}_{ij}(s)$$

$$\{i, j, k\} \in [1,3]$$

Equation 2.4

It is more convenient to write the equations describing linear viscoelasticity in the frequency (or Laplace) domain, as shown in Equation 2.4. This allows the correspondence principle to be applied. The correspondence principle enables the quasistatic viscoelastic solution of a stress analysis problem to be obtained from the elastostatic solution by replacing the time independent parameters in the elastostatic solution by the corresponding Laplace transforms (Tschoegl 1989).

Using the correspondence principle, the linear elastostatic solution to the cylindrical punch indenting a semi-infinite half-space, represented by Equation 2.1 (a) and Equation 2.1 (b), can be transformed to the linear quasistatic viscoelastic solution, represented by Equation 2.5 (a) and Equation 2.5 (b).

$$\frac{\bar{F}_z(s)}{\bar{\delta}_z(s)} = \frac{8a\bar{G}(s)\left[3\bar{K}(s) + \bar{G}(s)\right]}{3\bar{K}(s) + 4\bar{G}(s)} \qquad\qquad \frac{\bar{F}_x(s)}{\bar{\delta}_x(s)} = \frac{16a\bar{G}(s)\left[3\bar{K}(s) + \bar{G}(s)\right]}{3\left[3\bar{K}(s) + 2\bar{G}(s)\right]}$$

Equation 2.5 (a)   Equation 2.5 (b)

23

$$\frac{\overline{F}_z(s)}{\overline{\delta}_z(s)} = \frac{8a\overline{G}(s)\left[3\overline{K}(s) + \overline{G}(s)\right]}{3\overline{K}(s) + 4\overline{G}(s)}$$

$$\frac{\overline{F}_x(s)}{\overline{\delta}_x(s)} = \frac{16a\overline{G}(s)\left[3\overline{K}(s) + \overline{G}(s)\right]}{3\left[3\overline{K}(s) + 2\overline{G}(s)\right]}$$

<center>Equation 2.5 (a)</center>

<center>Equation 2.5 (b)</center>

The transfer functions represented in Equation 2.5 (a) and Equation 2.5 (b) are evaluated at discrete frequencies. For this particular set of experiments, both the force output and the displacement input are sinusoids. This means that the transfer function at a specified frequency is a complex number with a magnitude equal to the ratio of the two amplitudes and a phase equal to angle between the two sinusoids. Figure 2.2 shows this relationship.
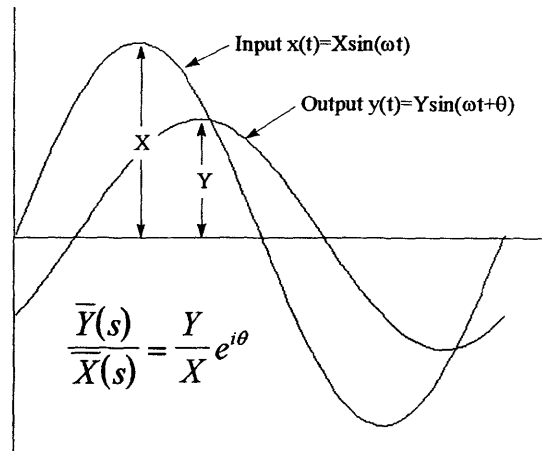
<center>Figure 2.2: Transfer Function Representation for
Sinusoidal Inputs and Sinusoidal Outputs</center>

It is now convenient to redefine the transfer functions in Equation 2.5 (a) and Equation 2.5 (b) as shown in Equation 2.6 (a) and Equation 2.6 (b). $N(s)$ and $T(s)$ represent complex numbers that vary as a function of frequency.

$$N(s) = \frac{\overline{F}_z(s)}{\overline{\delta}_z(s)}$$

$$T(s) = \frac{\overline{F}_x(s)}{\overline{\delta}_x(s)}$$

<center>Equation 2.6 (a)</center>

<center>Equation 2.6 (b)</center>

Simultaneously solving Equation 2.5 (a) and Equation 2.5 (b) in conjunction with the substitute variables introduced by Equation 2.6 (a) and Equation 2.6 (b) leads to the

determination of two elastic impulse response material functions, $\overline{G}(s)$ and $\overline{K}(s)$, at the specified discrete frequencies (De 1998). These frequency dependent material functions are given in Equation 2.7 and Equation 2.8.

$$\overline{G}(s) = \frac{N(s)T(s)}{4a[2N(s) - T(s)]}$$

$$\overline{K}(s) = \frac{N(s)T(s)[4N(s) - 3T(s)]}{6a[3T(s) - 2N(s)][2N(s) - T(s)]}$$

<div align="center">Equation 2.7   Equation 2.8</div>

From this point forward, this work uses the impulse response material functions, the shear modulus $\overline{G}(s)$ and the bulk modulus $\overline{K}(s)$, to describe the linear viscoelastic behavior of the human fingerpad tissue.

CHAPTER 3

THE TACTILE STIMULATOR

3.1 Hardware Requirements

In general, this device must provide vibrational indentations to the fingerpad. Specifically, the tactile stimulator must allow force or displacement inputs to be ramp-and-hold, sinusoidal, or noise wave forms. The frequency capabilities must be between 1 Hz and 300 Hz and the indentation depth must not exceed 3 mm. Also, the tactile stimulator must measure both forces and displacements while using a displacement controlled setup. Finally, the device must allow interchangeable indentors. With these specifications in mind, an existing device was replicated and modified to meet these specific needs.

3.2 Overview of the Tactile Stimulator

The tactile stimulator is a replication and modification of the TACTUATOR, developed by Hong Tan (1996). This machine was initially designed as an alternative sensory communication channel for deaf-and-blind individuals Although the original use of this machine is not directly related to this research, readers can find application information in Tan's doctoral thesis (1996).

The tactile stimulator provides one-degree-of-freedom indentation stimuli to the human fingerpad in the form of sinusoids, random signals, step functions, or ramps. Any indentor shape can be attached to the device to provide stimulation in either the normal direction or the tangential direction. The stimuli are position controlled and both displacement and force responses are measured. The stimulator operates smoothly in the range of 0.1 Hz to 300 Hz. Positions can be resolved to 0.8 µm while forces can be resolved to 0.8 mN. Figure 3.1 shows a photograph of the tactile stimulator with the key elements identified.
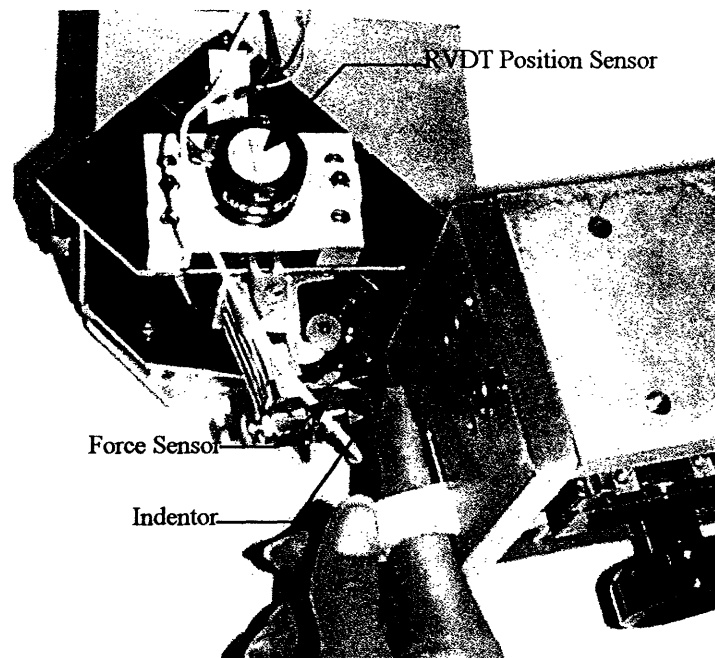
Figure 3.1: Photograph of the Tactile Stimulator

The main component of the tactile stimulator is a disk drive head positioning motor. A high precision actuator is attained by coupling this motor with angular position feedback from a precision rotary variable differential transformer (RVDT). The angular position data are collected through an A/D card on a personal computer. The computer's A/D card is also used to acquire force response data that is sent from the force sensor via a piezoelectric transducer.

The computer houses a floating-point digital signal processing (DSP) system that is used to implement a digital, real-time PID (proportional + integral + derivative) controller. The

processor compares a reference voltage to the actual position to derive a command input. The controller sends the command signal to the motor via a D/A converter and power amplifier. A signal flow diagram that includes all the components of the tactile stimulator is given in Figure 3.2.
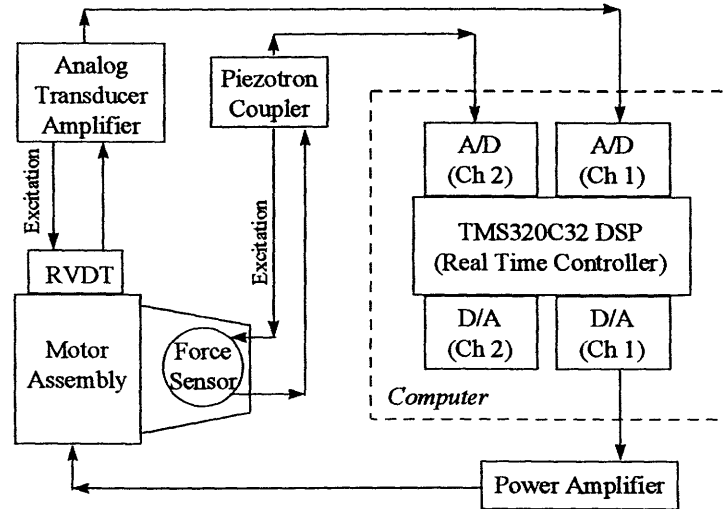
Figure 3.2: Signal Flow Diagram of the Tactile Stimulator System

3.3 Hardware Components

All system components from Figure 3.2 are described in further detail in this section. An overview of the design considerations for each component is also included.

3.3.1 Position Sensor

The selected position sensor is the same as the position sensor used in the original device, the TACTUATOR. The sensor is a Lucas Schaevitz R30A rotary position sensor. The R30A is an RVDT (Rotary Variable Differential Transformer) that measures the angular displacement of a rotating element. Although the measurement needed is actually a linear displacement, the small displacements that are commanded at the end of the armature coincide with the angular displacements. In fact, for a displacement of 1mm, the error from making the small angle approximation to the linear distance is less than 35 nm, which

is an order of magnitude smaller than the level of noise in the system. The small angle assumption for this case will be fully characterized in Section 3.5.

Other options explored for the displacement sensor include laser systems, LVDTs, and eddy-current displacement measuring systems. Laser systems would have given better accuracy, but they were considerably more expensive. LVDTs and eddy-current systems rely too much on the assumption that the system has perfectly linear motion. With the tangential component of angular displacements, either system might be easily damaged. After exploring these options, the RVDT seemed to give the highest accuracy for a reasonable cost. The RVDT will also be very durable in this application with a virtually infinite mechanical life.

This particular rotary sensor was chosen for several reasons. First, the sensor has a nearly infinite resolution due to the electromagnetic coupling of the mechanical input to the electrical output. Also, the unit has no rubbing contacts, allowing virtually frictionless and noiseless operation. The linearity is excellent for this sensor as well (0.17% of full scale displacement, factory calibrated). Finally, the sensor has a small and compact design that easily fits on the supporting structures for the disk drive. Specifications for the Lucas Schaevitz R30A RVDT are found in Table 3.1.

Table 3.1: RVDT Specifications

Specification	Value
Range	± 30°
Sensitivity	2.85095 mV/V/°
Linearity	± 0.17%
S/N	5099
Null Position	0.66 mV AC
Primary Impedance	370 Ω
Phase Angle	+3 degrees
Diameter	27 mm
Height	22 mm
Weight	36 grams

Mounting the displacement sensor (RVDT) requires a special procedure to ensure that the correct displacements are recorded. The center of the actuator bearing is actually stationary while the armature moves; therefore a mechanical link is required to convert the displacement of the armature to the sensor shaft of the RVDT. Furthermore, it is essential that the core of the RVDT is at the center of the armature pivot point. Tan (1996) designed four custom parts to assist in mounting the sensor. The parts are fully described in her dissertation, but they merit description here as well. The four mounting aids include a dummy sensor, a sensor support, a motion link, and two sensor fixtures. The dummy sensor is a replica of the RVDT; however, a longer threaded shaft protrudes to allow the dummy sensor to be screwed into the actuator bearing. The dummy sensor has the exact dimensions of the R30A, except for this special shaft. The dummy sensor ensures that the actual sensor will be co-concentric with the actuator. After the dummy sensor is in place, the sensor support is permanently fixed to the disk drive casing. The sensor support was designed so that the actual sensor is mounted in the correct position above the actuator bearing; however, the support still allows the actual sensor to be rotated so that the null position can be adjusted. After the sensor support is fixed and the dummy sensor is removed, the R30A can be placed in the fixture and the sensor shaft is co-concentric with the actuator bearing. The third component, the motion link, is simply a mechanical link that translates movement of the armature to angular motion about the shaft of the sensor. Finally, the two sensor fixtures are added to stabilize the sensor body after the null position has been adjusted. After following these mounting procedures, the RVDT measures the correct displacements without damage to the sensor.

Another essential component for the position sensing system is the Lucas Schaevitz ATA-101 Analog Transducer Amplifier. This is a power-line-operated instrument that provides excitation, amplification, demodulation, and DC power functions for the RVDT. The necessity of each of the four functions above will be described in detail and an overview of the ATA-101 in given in Table 3.2. The values in Table 3.2 reflect the characteristics of the ATA-101 instrument after all internal adjustments were made and the full scale output was adjusted appropriately.

Table 3.2: ATA-101 Analog Transducer Amplifier Specificaitons

Specification	Value
Transducer Excitation Amplitude	3 V rms
Transducer Excitation Frequency	10 kHz
Analog Filter Cutoff Frequency	1 kHz
Input Impedance	100 kΩ
Output Impedance	< 2 Ω
Full Scale Output	± 3 V DC
Sensitivity	5000 mV rms/10 V DC
Nonlinearity	< ±0.05% Full Scale Output
Weight	0.8 kg

Excitation is essential to operate the RVDT. The RVDT requires a constant amplitude AC input at a frequency not readily available. This means that an oscillator of the appropriate frequency must be connected to an amplifier with amplitude regulation on its output. The unit is supplied with a 2.5 kHz excitation frequency module installed. This module also has a low pass output filter with a cutoff frequency of 250 Hz. For this specific application, a higher cutoff frequency is needed to allow the unit to collect displacements accurately at higher frequencies. A 3.5 kHz/350 Hz module is ideal; however, the only other module option has a 10 kHz excitation frequency and a 1 kHz cutoff frequency for the output filter. The higher excitation frequency is advantageous because it increases the sensitivity of the RVDT. The excitation frequency was finally set to 10 kHz to achieve a 1 kHz nominal -3 dB bandwidth. After installation of the excitation/filter module, the amplitude of the excitation signal is adjusted to be 3 V rms, as required by the RVDT.

Amplification of the signal from the RVDT is also an essential function performed by the ATA-101 instrument. The RVDTs output has such a low level that a precision readout cannot be obtained without amplification. The ATA-101 comes from the factory with a gain setting of one. This is not sufficient for this particular application, considering the full scale range for this particular application in conjunction with the RVDTs sensitivity. The two internal gain selection jumpers were adjusted to provide a gain of 10 for the RVDT output signal. This is the highest gain possible for this instrument.

Demodulation is another critical function that the ATA-101 provides for the RVDT. The position signal sent to the computer should be a DC signal, but the amplified output from the RVDT is an AC signal. The demodulator converts the AC signal to a DC signal.

Finally, the ATA-101 provides DC power for all of the electronic circuits. All of the circuits in the position sensor and ATA-101 require stable DC voltages for proper operation.

A block diagram of the interaction of the RVDT and the ATA-101 instrument is given in Figure 3.3. This figure also gives an overall view of the position sensing system. The diagram serves two purposes: to depict the main internal functions described above and to show how the RVDT relies on the ATA-101.
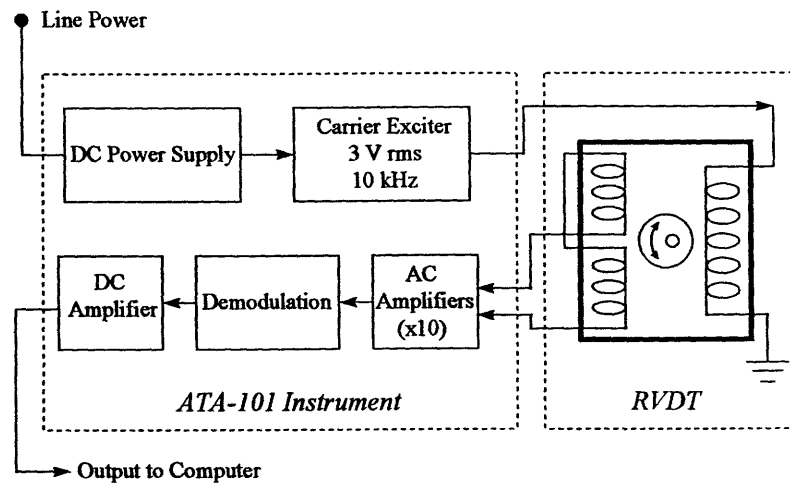

Figure 3.3: The Position Sensing System

The RVDT was configured to limit the range of motion to 4.3 mm. This allows better accuracy and resolution in the overall range of movement of the RVDT. Full scale output is set to ±3 V, which is dictated by the voltage limits of the A/D card mounted on the DSP board. Calibration of the position sensor is discussed in Section 3.4.

3.3.2 Force Sensor

The choice of a force sensor for the tactile stimulator was a key design issue for the device. Three strict requirements were imposed on the force sensor selection process. First, the deflection of the force sensor must be no more than 1 μm for the maximum expected load of approximately 2 N. This requirement precludes diminishing the accuracy of the displacement sensor and controller. Secondly, the force sensor must be lightweight and compact to avoid decreasing the performance of the tactile stimulator by adding significant inertial loads to the motor. Finally, the force sensor must have a resolution that is better than 10 mN. Several possibilities for the force sensor were considered with these requirements in mind.

Several strain gage based force sensors were explored and eventually rejected. The displacement requirements ruled out a traditional force sensor based upon strain gages mounted on a cantilever beam subjected to strains from forces and moments. Beam deflection analyses for a variety of beam geometries indicate that deflections would occur that are more than an order of magnitude greater than the maximum allowable deflection. Furthermore, the geometry of these sensors would significantly affect the inertial properties of the device, resulting in decreased motor performance. The octal ring configuration suggested by Cook *et al.(1963)* is another strain gage based force sensor that was considered. The ring configurations deflect less than the cantilever geometries, but the deflections are still much too large for the stringent displacement requirements. Also, as the geometries change to decrease deflections, the sensor becomes nearly impossible to machine. Finally, the configurations that approach acceptable levels of deflection do not have adequate surface areas for mounting strain gages. In lieu of strain gage based force sensors, an alternate strategy is preferred.

A piezoelectric load cell was selected as the force sensor for the tactile stimulator. This load cell has a sensing element of stacked crystalline quartz wafers assembled under an initial static compression preload greater than 2200 N. This configuration allows the cell to be very rigid, resulting in negligible deflections for small forces. The selected force

sensor deflects less than 5 nm for a 2 N load. Additionally, piezoelectric load cells are compact and light. The selected load cell weighs only 18 grams. Piezoelectric load cells are designed to measure dynamic and short-term static forces, which is ideal for this particular application. Furthermore, these load cells are very sensitive in both tension and compression and have a very fast response. The drawback of this type of force sensor is the tendency of the sensor to act as an accelerometer. This problem will be dealt with in Section 5.2.

The selected load cell is a Kistler 9712A5 quartz piezoelectric load cell. The characteristics of this specific load cell can be found in Table 3.3. This load cell embodies a built-in solid-state impedance converter that changes the high impedance sensing element signal into a low impedance analog voltage output. This load cell is designed to measure dynamic compression and tensile forces. Forces applied along the sensitive axis are converted by the quartz-wafer sensing element into a proportionate electrical charge signal.

Table 3.3: Load Cell Specifications

Specification	Value
Range	± 22.24 N
Threshold	± 0.9 mN
Sensitivity	868 mV/N
Linearity	± 1%
Rise Time	< 6 µs
Time Constant	260 s
Rigidity	1.1 nm/N
Overload Capacity (Compression)	110 N
Full Scale Output Voltage	4.5 V
Weight	18 grams

In addition to the load cell, a power supply/coupler is necessary to complete the force measurement system. The power supply/coupler is a solid state instrument that carries out three important functions. First, the coupler provides the constant current and voltage required by the low impedance sensor. Additionally, it houses an amplifier, a lowpass filter, and a highpass filter. The power supply/coupler is configured so that the gain and

the highpass filter cutoff frequency (-3 dB) can both be configured from the front panel of the power supply/coupler. The lowpass filter, however, is not factory installed. The plug-in module to implement the desired 500 Hz lowpass filter is integrated into the instrument in the laboratory. Finally, the power supply/coupler serves another useful purpose: monitoring the bias voltage which reflects the condition of the sensors and cables. The power supply/coupler chosen for this application is a Kistler 5118A Power Supply/Coupler. Specifications for this instrument are shown in Table 3.4.

Table 3.4: Power Supply/Coupler Specifications

Specification	Value
Gain	10
Frequency Response (-3dB)	0.006 Hz to 500 Hz
Output Impedance	100 Ω
Time Constant	5.25 s
Full Scale Output Voltage	± 5 V
Noise	< 2 mV rms
Null	-0.8855 μN
Weight	0.45 kg

The final task in successfully implementing the force sensor is mounting the load cell properly. As with the position sensor, special care must be exercised when mounting the force sensor. Flatness and smoothness are essential for the two surfaces between which the load cell is mounted. For this device, both surfaces were machined to be flat to 2 μm and smooth to 400 nm. The load cell must also be mounted by invoking tension in the mounting studs. These studs should never touch the bottom of the load cell. Following these criteria allows for the proper transmission of forces and prevents stress concentrations that can lead to crystal fracture.

3.3.3 Motor Assembly

The actuator used for the tactile stimulator is the head-positioning motor from a Maxtor hard-disk drive. The head-positioning motor from a hard-disk drive is ideal for this application for two reasons: it has a wide bandwidth and it operates smoothly at very low frequencies.

Several modifications were made to the motor assembly to prepare it for this specific application. First, the drive was stripped of all electronic components. Next, the original casing was cut so that only the head-positioning motor and its bearing and supporting structures remain. The position sensor, the force sensor, and the indentation interface were designed around the remaining structure. As discussed earlier, this actuator configuration forces special mounting procedures for the RVDT angular position sensor. A special assembly was designed to provide a place to mount the force sensor and indentor at the end of the armature. This assembly utilizes the armature configuration to provide a stable mounting surface for these two components. The overall assembly was mounted on a V-shaped block with vibration absorbing pads on the underside. Refer to Figure 3.1 for a photograph of the hardware.

Two electrical connections integrate the disk drive motor with the other components of the tactile stimulator. First, the leads on the motor (ground and signal) are connected to the output of the power amplifier. This allows the computer's command signal to be sent to the disk drive motor. The second connection provides power to the disk drive. This set of leads is connected to a 5 V constant voltage power source. This power does not drive the motor, rather it unlocks the armature of the motor. Once the armature is unlocked, the actuator can move freely between the two built-in mechanical stops. These mechanical stops physically limit the range of motion of the armature to slightly less than 30°.

One final modification improves the utility of the tactile stimulator. Two more mechanical stops are added to the device to restrict the motion of the device even further. Further restriction of the armature ensures avoidance of excessively deep indentations of the fingerpad. Physical barriers (small blocks of metal) are placed in the space between the position sensor mount and the disk drive cover. When present, these barriers limit the range of motion of the indentor to the specific range of the experiments.

An electromechanical model of the motor was found by Tan when she designed the original device, the TACTUATOR. Her dissertation (1996) shows complete details. A

summary of the model follows here, along with a replica of her pictorial representation. Figure 3.4 is a schematic diagram of the armature-controlled DC motor.
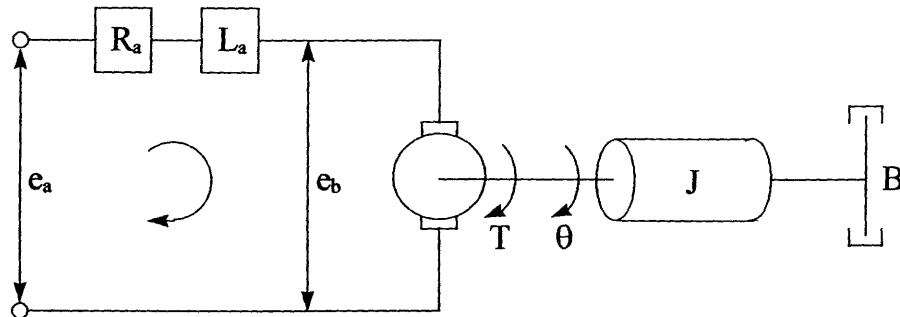

Figure 3.4: Schematic of the DC Motor

The torque delivered by the motor (T) is proportional to the input current. The motor torque constant (K) is the ratio of the torque delivered by the motor (T) over the input current (i_a). Tan (1996) estimated the torque constant (K) to be 0.2 N·m/A by placing known weights at the end of the arm and measuring the input current (i_a) needed to hold the weight up. The armature winding has a small resistance, R_a. An LCR meter indicates that R_a is 4 Ω. The armature winding also has a small inductance, L_a, which was measured to be 0.3 mH. Another parameter that gives the characteristics of the motor is the back emf constant (K_b). The back emf voltage (e_b) is proportional to the angular velocity ($d\theta/dt$) of the motor. The ratio of the back emf voltage (e_b) over the angular velocity ($d\theta/dt$) of the motor is the back emf constant (K_b). When metric units are used, $K_b = K$. The equivalent moment of inertia (J) and the equivalent viscous-friction coefficient (B) were not measured.

3.3.4 Power Amplifier

A power amplifier is necessary because the signal coming out of the computer does not have enough power to drive the hard-disk drive head positioning motor. A Crown D-150A amplifier provides the additional power that the computer's controller signal needs. This amplifier is the same model that Tan used for the original device. This amplifier is ideal for the tactile stimulator because of its smooth frequency response and low phase distortion the range of interest (0 Hz to 300 Hz). Also, the disk drive head

positioning motor has a typical resistance of 4 Ω and a very small inductance of 0.3 mH. Since the amplifier is designed to drive loudspeakers, and the motor parameters are similar to those of loudspeakers, this amplifier works well for the tactile stimulator. Another advantage of the Crown D-150A amplifier is that it is not pulse-modulated; therefore, it introduces very little noise or harmonic distortion, which is important in this high precision application. Pertinent specifications of the Crown amplifier can be found in Table 3.5.

Table 3.5: Amplifier Specifications

Specification	Value
S/N	110 dB
Frequency response(DC to 20 kHz)	±0.1 dB
Phase Response (DC to 20 kHz)	+0° to -1°
Harmonic Distortion	<0.001%
Rated Load Impedance	16 Ω
Damping Factor (DC to 400 Hz)	> 400
Weight	11 kg

For all experiments, the gain of the power amplifier is set to one. This ensures that the signal sent to the motor will always be in the range of ±3 V (the same as the range of the signal coming from the D/A board in the computer).

3.3.5 DSP Board and I/O Devices

The DSP board and the I/O devices facilitate two essential functions: data collection and controller implementation. The signal processing equipment is housed in a PC with a 486 MHz processor. The main component of this equipment is the Spectrum C32 Real-time System board. This is where the data are stored and where the calculations for the controller are performed. The system board also includes a daughter module site where the Spectrum 16-bit 200 kHz Daughter Module resides. The daughter module serves as an analog signal interface for the system board by implementing the A/D and D/A converters. Both components, the system board and the daughter module, are explained fully in this section.

The Spectrum C32 Real-time System board is an IBM PC-compatible card based on the Texas Instruments 50 MHz TMS320C32 floating-point processor. Highlights of the PC board can be found in Table 3.6.

Table 3.6: Spectrum C32 Real-Time System Board Specificaitons

Specification	Value
Processor	50 MHz floating-point
Instruction Cycle Time	40 ns
On-Chip RAM	512k x 32
CPU	32/40-bit floating-point
On-Board External Memory	256k x 32
Daughter Module I/O Sites	2
PC Interface Bus	8/16-bit
PC Interface Data Transfer	Memory-Mapped Dual Port SRAM

One of the main advantages of this particular system board is the flexibility of the memory configuration. The main memory on the board is arranged in two continuous areas that can be accessed as 8, 16, or 32-bit words. For this application, both memory banks are used and the entire main memory is configured (through software) to be accessed as 32-bit words. Both banks can hold a variety of sizes of zero wait-state SRAM. Currently, both banks of the board are filled with 128k x 32 zero wait-state SRAM. This board also has a 32k x 8 EPROM. The EPROM contains code that allows transfer of application programs from the PC host to the board via DPRAM. The EPROM is accessed at power-up or reset so that the board can be used in embedded stand-alone real-time applications.

The C32 system board also has a convenient PC host interface. A fast interface is provided by using 2k x 16 DPRAM that is mapped into both the C32 board and the PC host memory spaces. Several software-configurable registers are also mapped into the PCs I/O location. These resources also allow bi-directional interrupts between the C32 board and the PC.

A final important feature of the system board is the I/O capabilities. Several I/O options are available for this particular board; however, only the daughter module sites are discussed here, as the other options are not utilized for this project. The C32 system

board has two AMELIA daughter module sites. Only one site is used in this application. The daughter module is a Spectrum 16-bit 200 kHz daughter module. A summary of the features of this module can be found in Table 3.7.

Table 3.7: Spectrum Daughter Module Specifications

Specification	Value
Number of Input Channels	2
A/D Converters	16-bit, 200 kHz
Input Voltage Range	± 3 V
Input Impedance	20 kΩ
Input S/N	82 dB
Number of Output Channels	2
D/A Converters	16-bit, 400 kHz
Output Voltage Range	± 3 V
Output Impedance	0.5 Ω
Output S/N	86 dB

This dual-channel daughter module uses Burr-Brown 16-bit successive-approximation A/D converters on both input channels for sampling frequencies up to 200 kHz. For this application the sampling rate is set to 4 kHz, well above the maximum operational frequency of 200 Hz. The input channels also include sample-and-hold amplifiers. Both input and output channels are equipped with 4th order active Butterworth filters and low-noise buffering. Finally, inputs and outputs are both limited to a range of ±3 V. This limits the output to the amplifier to this range. Inputs from both the force and position sensors must be within this range as well.

The real-time DSP board is a flexible device that has been tailored to the needs of this particular application. Most of the options for the board can be configured using software. Furthermore, the board can be expanded to meet more demanding needs by adding more on-board memory or by adding additional daughter modules to increase the number of I/O channels. The flexibility of the board, along with its real-time capabilities, made the C32 system board the top choice for this application.

3.3.6 PID Controller

The tactile stimulator is controlled by a digital PID (proportional, integral, and derivative) controller. An initial guess for the controller parameters can be determined by using the Ziegler-Nichols (1942) stability-limit rules for tuning PID controllers. These tuning rules are aimed at obtaining 25% maximum overshoot. The form of the digital controller is given by C(z) in Equation 3.1, where K_P, T_I, and T_D are respectively the proportional, integral, and derivative controller parameters to be determined, T is the sampling period (0.25 ms), and z is the z-transform variable.

$$C(z) = K_p \left(1 + \frac{Tz}{T_I(z-1)} + \frac{T_D(z-1)}{Tz} \right)$$

Equation 3.1

To begin parameter estimation using the stability-limit method, T_I is set to infinity and T_D is set to zero, leaving only the proportional term. K_p is now gradually increased from zero to a critical value, K_{cr}, where the output first exhibits sustained oscillations. The oscillation period at this gain is recorded as P_{cr} in seconds. Table 3.8 shows the initial values for the controller parameters based on the experimentally measured parameters, K_{cr} and P_{cr}. For the tactile stimulator, $K_{cr} = 1.3830$ and $P_{cr} = 43.0$ ms.

Table 3.8: Controller Parameters Using the Ziegler-Nichols Tuning Method

	K_p	K_I	K_D
Ziegler-Nichols Formulation	$\frac{3}{5}K_{cr}$	$\frac{1}{2}P_{cr}$	$\frac{1}{8}P_{cr}$
Ziegler-Nichols Values	0.8298	0.0215 s	0.0054 s
Final Controller Values	0.6640	0.0269 s	0.0043 s

Although the Ziegler-Nichols tuned controller is acceptable for most applications, the tactile stimulator requires a controller with particularly low overshoot because it is important not to indent the fingerpad too deeply. The controller was fine-tuned to enhance the transient response of the overall device. The final controller values are found in Table 3.8. Adjusting the controller involves trade-offs; in this case, the main compromise is between a fast steady state value and the maximum amount of overshoot. Both are important as real-time control is desired, but too much overshoot can lead to invalid fingerpad responses. Methods for adjusting the Ziegler-Nichols initial parameters to meet the needs of a particular system are discussed extensively in the literature (Ziegler and Nichols 1942, Ogata 1997, Parr 1996). More complicated controllers, such as self-tuning controllers, could be implemented to improve the performance of the system. In this case, a simple PID controller is used.
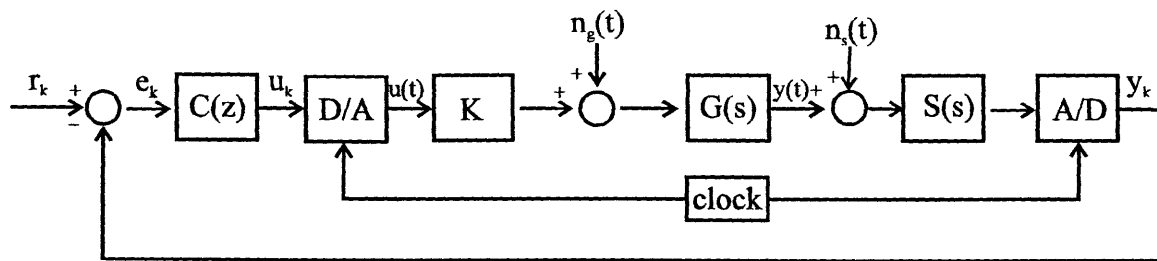
Figure 3.5: Signal Flow Diagram Representing Position Control

Figure 3.5 shows the signal flow diagram for the overall position control system. The blocks represent the transfer functions for various system components. $C(z)$ is the controller, D/A is the digital to analog converter, A/D is the analog to digital converter, K is the gain of the amplifier, $G(s)$ represents the analog plant or motor dynamics, and $S(s)$ represents the analog position sensor dynamics. The circles represent signal summation blocks. The signals depicted are as follows: r_k is the desired position, e_k is the digital error signal, $u(t)$ is the commanded analog position signal, $n_g(t)$ is noise input to the motor system, $y(t)$ is the actual position of the motor armature, $n_s(t)$ is noise input to the position sensing system, and y_k is the recorded position. Note that the clock is synchronized between the D/A and A/D converters.
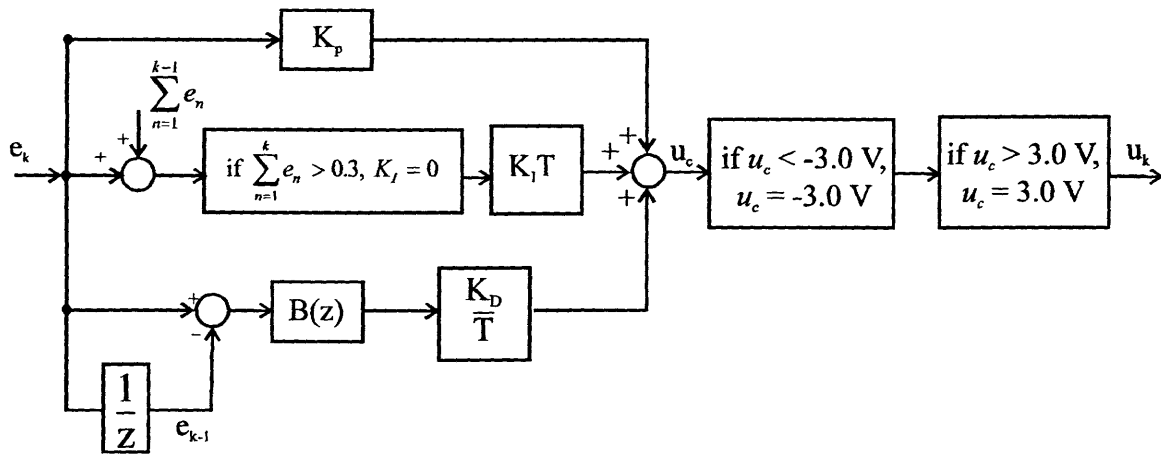
43

Figure 3.6: Signal Flow Diagram of the Controller

Figure 3.6 shows a detailed signal flow diagram of the controller, represented by the transfer function block $C(z)$ from Figure 3.5. This diagram shows that the PID controller is a summation of three terms. The proportional term of the controller is simply $K_p e_k$. The integral term of the controller is $K_i T \sum e_k$, where T is the sampling period (0.25 ms) and $\sum e_k$ is the summation of all previous error signals. Note that the integral term is set to zero when the magnitude of the summation of the errors is larger than 0.3 V. The differential term of the controller is $v_k K_D/T$, where v_k is the filtered velocity estimate. The velocity estimate is represented by v'_k where $v'_k = e_k - e_{k-1}$. In Figure 3.6, the transfer function block, $B(z)$, represents a digital Butterworth filter that is necessary to smooth the velocity signal. The difference equation for the 300 Hz lowpass Butterworth filter is given by Equation 3.2.

$$v_k = 1.3490 v_{k-1} - 0.5140 v_{k-2} + 0.0413 v'_k + 0.0825 v'_{k-1} + 0.0413 v'_{k-2}$$

Equation 3.2

3.3.7 Computer Software

Custom-tailored computer software is essential for the tactile stimulator to operate properly. The software for the tactile stimulator consists of two threaded programs: a C32 system board resident program and a host PC resident program. The system board

resident program provides for the operational aspects of the tactile stimulator, including the controller. The PC resident program controls the automatic flow of the experiments, sends the appropriate parameters to the DSP board, and creates MATLAB binary output data files. Due to the length of these programs, they will not be included in this dissertation, but the key elements of the programs will be discussed further here.

Software development tools assisted in the code generation process for the tactile stimulator. Host DOS and Windows interface libraries, along with an I/O utility, automatically generated much of the low-level code (assembly language) required to configure the DSP board and implement the application. These tools are useful for developing both the PC resident program and the DSP board resident program.

Another important debug environment provided with the DSP board is MPC View. MPC View is a Windows 3.1 based C source level tool that allows debugging in both C and assembly language. The nature of the threaded programs for this application make this debugger essential for developing the code that is resident on the C32 system board; otherwise the C32 code could not be executed without the use of PC resident code. This debugger also allows the user to look directly at the memory of the DSP board. This option is quite useful in analyzing where data transfer problems might exist. Data must be collected on the DSP board, sent to the DPRAM, transferred to the host PC, and finally, written to a binary file. This inside view of the system memory at any point in time helps to narrow down the source of any unexpected data. In many ways, this debugger is essential for developing executable code for the tactile stimulator.

3.3.8 Finger Support/Constraint Device

The finger support/constraint device is detached from the tactile stimulator. The constraint is based upon a precision horizontal displacement stage. This stage allows the experimenter to place the fingerpad in the desired location with a high degree of precision (~2.5 μm). The horizontal stage has been modified to allow the subject rest his or her arm on the table while the middle finger of the right hand is supported by the stage. Figure 3.1 shows a small part of the support device.

The stage is oriented so that the palm of the hand is in the vertical plane. Slots were cut on the constraint device to allow a Velcro strap to secure the middle joint of the finger to the platform. Foam padding was included behind the fingerpad so that the knuckle was not resting against the steel during the experiments. Additionally, a looped strip of padding is located above the Velcro. This secures the index finger, allowing the subject to rest the index finger during the experiments without interfering with the tactile stimulator. Finally, a portion of the support/constraint device is designated for gluing the fingernail to the platform.

It is clear from the experimental data that this support/constraint device is successful for immobilizing the fingerpad of the subject during the course of the experiments. The procedure for mounting the fingerpad on the support/constraint device is discussed in the next chapter.

3.4 Calibration

Calibration of the displacement measuring system is essential to obtaining accurate experimental data. Because the tactile stimulator is a high precision device, simple calibration blocks or shims are not adequate. The position sensor was calibrated using a laser Doppler vibrometer. The laser Doppler vibrometer can detect movements smaller than 1 nm. The precision of the position sensor can be estimated from factory calibration data to be on the order of 1 μm, therefore this system is adequate to calibrate the position sensor. More than 750 displacement locations were commanded in a pseudo-random fashion by the software while the position sensor signals and laser Doppler vibrometer signals were acquired by the DSP board. This method of calibration allows three factors to be lumped within one conversion factor. The factors affecting the conversion factor include the effects of the dynamics of the displacement sensor, the effects of the A/D board, and the effects of conversion of angular displacement to linear displacement.

The force sensor was calibrated in the factory with a signal conditioner exhibiting a gain of 10 (as with the tactile stimulator system). Only short-duration static measurements can be accomplished due to the nature of piezoelectric devices. The measurements must be

within the limits of the system time constant, which is a function of the time constants of both the load cell and the coupler. A limited number of data points quickly confirmed the accuracy of the factory calibration.

Overall results of both calibrations are summarized in Table 3.9. Note that rms (root mean square) noise is typically defined as the resolution in the literature. The true meaning of this term is that 68.2% (± 1 standard deviation) of the noise will fall within this limit. The rms value is multiplied by the desired number of standard deviations to calculate the value within which at larger percentage of the noise falls. A brief analysis of the noise indicates that the noise in the position sensor has a clear trend while the noise in the force sensor approximates pure noise. Since the precision of the machine is within the desired range, no further investigations were performed to find of the source of the noise trend in the displacement sensor.

Table 3.9: Calibration Results

	Displacement Sensor	Force Sensor
Conversion Factor	$\dfrac{717 \; \mu m}{1 \, V}$	$\dfrac{514.44 \; mN}{1 \, V}$
Range of Sensor	4.302 mm	±1.537 N
RMS Noise	0.8 μm	0.8 mN
Peak to Peak Noise	2.5 μm	2.5 mN
Null Position	8 μm	-24.9 mN

3.5 Characterization of the Hardware

This section discusses three main characteristics of the hardware. First, a general model of the hardware performance is described. Next, additional factors that might influence the accuracy of the tactile stimulator are discussed. Finally, additional notes about the hardware are documented.

A model for the transfer function of the motor was developed using spectral methods described by Inman (1994). This modeling method leads to the transfer function represented by the Bode plot in Figure 3.7. This Bode plot represents the closed loop transfer function of the unloaded system. In other words, the controller and feedback loop with no fingerpad present are accounted for in this Bode diagram. Figure 3.7 indicates that the overall behavior of the tactile stimulator is similar to a lowpass filter. The bandwidth of the system is approximately 33 Hz. This does not mean that the system cannot perform well above 33 Hz, however. This simply indicates that an amplification factor is necessary for frequencies above 33 Hz. Note that the phase is plotted on a wrapped scale. Slight variations in the phase plot near 180° may look like phase jumps. Also, the phase plot is near 180°, as opposed to 0°, at low frequencies because the displacement is inverted during data processing in order to define normal indentations as positive displacements.
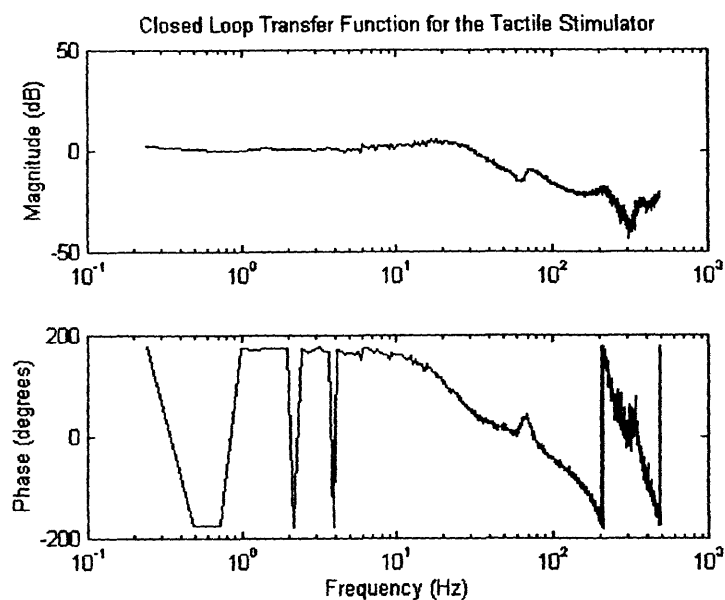
Figure 3.7: Bode Plot of the Closed Loop Transfer Function of the Tactile
Stimulator System

Since the controller was designed using a tuning method, an accurate dynamic model of the system is not necessary; therefore, no further work was completed on further characterizing the dynamics of the closed loop system.

Three separate issues concern the reliability of the displacement resolution: the compliance of the armature of the motor, the compliance of the force sensor, and the error due to the small angle approximation. None of these issues interfere with the resolution of the positions. Each is discussed separately.

The stiffness of the armature of the disk drive motor is a major consideration for the accuracy of the forces being measured at the base of the armature. If the armature deflects too much, the resolution of the positions being recorded is greatly reduced. A simple conservative model of the armature indicates the armature deflects approximately 0.4 μm at the end when a force of 2 N is applied to the end of the armature. The 0.4 μm deflection is about half the magnitude of the expected noise in the force sensor. Furthermore, the reaction forces exerted by the fingerpad are not expected to be greater

than 2 N. This conservative calculation shows that the deflection in the armature is small compared to the inherent noise of the system.

Another potential threat to the resolution of the position sensor is the compliance of the force sensor. The piezoelectric force sensor is designed to be quite stiff. With a force of 2 N, the force sensor deflects approximately 2 nm. This deflection is not detrimental to the precision readings of the position sensor.

The small angle approximation is the last system issue that could effect the resolution of the displacement sensor. There are two ways in which the small angle approximation could cause problems. First, the motion of the armature resulting in normal indentations may include large displacement errors. An analysis of this error reveals that the maximum expected error is on the order of 40 nm. Figure 3.8 shows how this error varies with commanded linear displacement.

Error in Normal Displacement Due to Angular Approximation
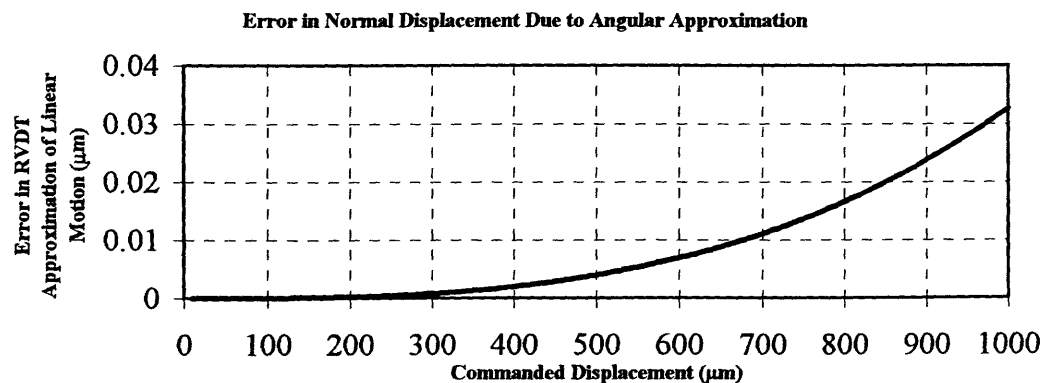
Figure 3.8: Quantification of the Error in the Normal Direction Due to the Small Angle Approximation

The other possible source of error from the small angle approximation is an undesired tangential motion. The error due to this approximation is plotted in Figure 3.9. Most of the displacements are on the order of 200 μm, which means the motion in the undesired direction will be less than 1 μm. Since the order of magnitude of this displacement with respect to the desired displacement is very small, this tangential motion is neglected.

Tangential Displacements Induced by Angular Motion
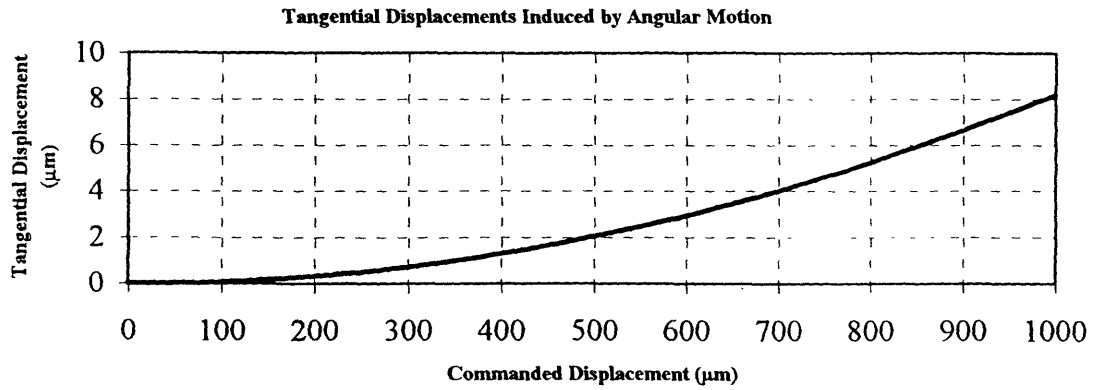
Figure 3.9: Quantification of the Tangential Motion of the Indentor when a Normal Motion is Desired

One final note is included on the nature of the hardware. The ATA-101 displacement transducer must be warmed up for a minimum of 30 minutes to function properly.

It is clear that the system components do cause errors in the measurements recorded by the displacement sensor, diminishing its precision. The errors mentioned in this section, however, are small compared to the measured noise levels. This indicates that the displacement sensor can be read without additional corrections.

CHAPTER 4

EXPERIMENTAL METHODS

The second phase of this research used the tactile stimulator, constructed in phase one to collect experimental data. The specifics of the stimuli are presented in Section 4.1. The hardware is discussed in Chapter 3, and the specifics of the experimental configuration are included in Section 4.2. The step-by-step protocol is not included in this dissertation, but the general procedure for preparing subjects is discussed in Section 4.3.

The experiments in this work were consistent with the rules and regulations established by the Massachusetts Institute of Technology Committee on the Use of Humans as Experimental Subjects. As required, each subject signed an informed consent document prior to commencement of the experiments.

4.1 Stimuli

The experiments are broken in to two basic categories: normal indentation stimuli and shear deformation stimuli. Both of these categories are comprised of two sets of data. The first set of data confirmed that the displacements are in the linear range. The second set of experiments gave the force-displacement data necessary to determine the mechanical

properties of the human fingerpad. All of the data that were collected to verify the linear range were also used to determine the mechanical properties of the human fingerpad.

Each trial had a given displacement controlled input, and both displacement and force response data were collected. Figure 4.1 shows the indentor configuration with respect to the fingerpad for experiments in both the normal and tangential directions. The symbols F_z and F_x represent the reaction forces of the fingerpad while δ_z and δ_x represent the displacements delivered by the probe.
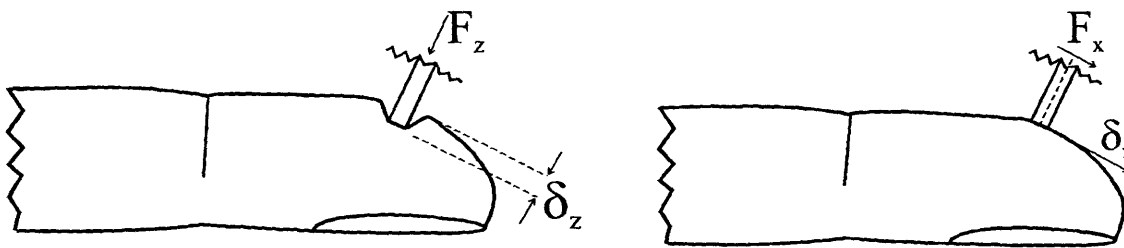
Figure 4.1: Normal Indentation (left) and Tangential Stretch (right)
Note: Figure not to scale

Each trial consisted of three phases: a ramp phase, a hold phase, and a stimulus phase. For the tangential experiments, the ramp phase was not necessary because the stimulus was applied the undeformed skin surface. A variety of frequencies in the range of 2 Hz to 200 Hz were used. A random signal was also used as a preconditioning stimulus. All stimuli were preceded by a 30 second hold to allow the fingerpad to reach a steady-state condition before the desired stimulus was applied. For the normal indentations, a preindentation was applied so that the tissue was not under tensile loading with respect to the resting surface of the skin. The preindentation depth was reached using a ramp speed of 8 mm/s. This slow ramp speed reduces overshoot, which is undesirable because the probe could indent the skin too deeply and increase the time required for the fingerpad tissue to reach a steady state value. All stimuli had a duration of 10 seconds. Ten seconds allowed the force response to reach a steady state, but is not so long that the subjects had to sit for long periods of time during experiments. Long duration stimuli would not produce more reliable steady state data because subjects cannot remain completely

motionless for long periods of time, reducing the accuracy of the data. Figure 4.2 gives description of the parameters used to define the stimuli.
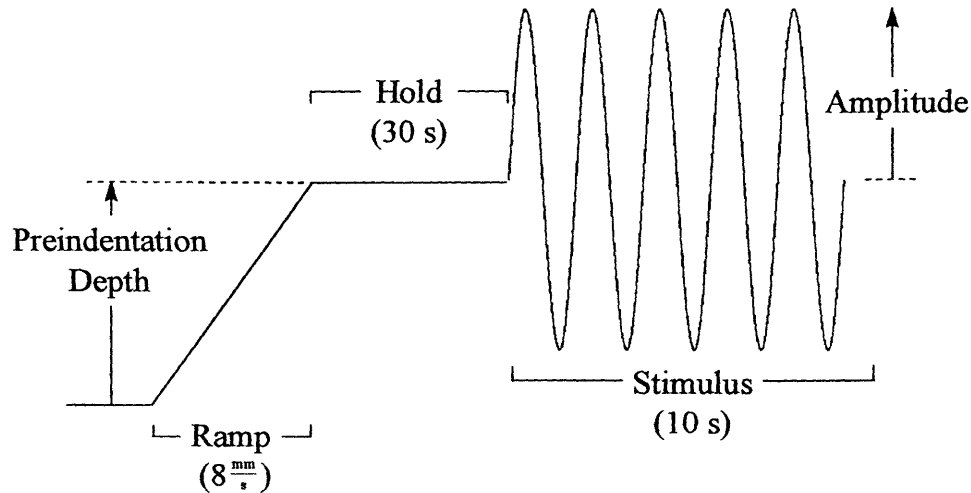
Figure 4.2: Description of the Stimulus Parameters
Note: This figure is not to scale.

The actual stimuli for the experiments in this work are listed in Table 4.1. Note that the experiments used to show linearity are also used to determine the mechanical properties of the human fingerpad. Theoretically, the linearity of the fingerpad tissue depends only on the displacement, not the frequency of the stimulus; however, linearity was checked at two different frequencies to experimentally show that this statement is true. Amplitudes of 50 μm, 100 μm, and 150 μm were chosen to verify linearity because they are convenient multiples within the linear range. Observing summations of the outputs verified that the superposition principle applies for this case.

Table 4.1: Experimental Stimuli

Frequency (Hz)	Normal Indentation Preindentation Depth: 200 μm		Tangential Stretch Preindentation Depth: 0 μm	
	All Stimuli	Stimuli Used for Linearity Check	All Stimuli	Stimuli Used for Linearity Check
	Amplitude (μm)			
2	50, 100		50, 100	
10	50, 100, 150	50, 100, 150	50, 100, 150	50, 100, 150
20	50, 100		50, 100	
40	100		100	
60	50, 100		50, 100	
80	100		100	
100	50, 100, 150	50, 100, 150	50, 100, 150	50, 100, 150
120	100		100	
200	50, 100		50, 100	

Several factors determined the frequencies at which data were collected. The capabilities of the tactile stimulator were the driving factors for which frequencies can be considered. The tactile stimulator is limited at the lower end of the spectrum by the capabilities of the force sensor. The minimum frequency that the force sensor can measure is approximately 0.5 Hz. At 200 Hz, the tactile stimulator, in a loaded condition, can deliver sinusoidal displacements with a maximum amplitude of 110 μm. Gulati and Srinivasan (1995, 1997) collected extensive data in the low frequency range, so the experiments in this work will start with a minimum frequency of 2 Hz. The chosen frequencies were spaced linearly as opposed to logarithmically because higher frequencies are of primary interest. Kárason *et al.* (1998) predicts that the mass of the fingerpad must be taken into account when displacement inputs exceed 175 Hz. Pawluk and Howe (1996a,b) assert that their model breaks down above 200 Hz due to the inertial effects of the fingerpad. A frequency of 200 Hz seems to be a logical upper limit because of the mass effects of the fingerpad in conjunction with the capabilities of the tactile stimulator.

The depth of the indentations for the normal load experiments was based on preliminary subject data and data collected by Gulati and Srinivasan (1995, 1997). Displacements

were small so that they did not invoke nonlinearities. From a data analysis (Srinivasan *et al.* 1998), it appears that the force-displacement response can be linearized for indentation depths of less than 1 mm. The depth of indentation plus the amplitude of the stimulus must therefore be less than 1 mm. To be safe, preliminary subject data included preindentation depths of 100 μm and 200 μm with amplitudes ranging from 20 μm to 150 μm. All data were linear, so the experiments proceeded using a preindentation depth of 200 μm in the normal direction. In the tangential direction, no preindentation was made so as to avoid material "pile up", which would corrupt the results of the tests. In the tangential direction, all of the amplitudes (20 μm to 150 μm) appeared to invoke linear behavior for the preliminary subjects. Linearity issues are discussed further in Chapter 5 and the results of the linearity tests are found in Appendix A.

The experiments were designed to reduce the time consumed by data collection while still retaining the randomness that leads to valid results. Kiemele *et al.* (1993) and DeVor *et al.* (1992) emphasize the necessity of randomness in the experimental order. On the other hand, Gulati and Srinivasan (1995, 1997) found that some order is necessary in the experiments to obtain repeatable data. Two sessions were necessary to collect all the data: a normal indentation session and a tangential deformation session; the order of each session of experiments was equivalent. Each of the stimuli listed in Table 4.1 was applied three times to get an average response of the fingerpad. The test schemes listed in Table 4.1 were randomized to determine the order of the experiments; however, the experiments were performed three times in this same order to obtain all of the desired data. The order of experiments maximized randomness while still producing repeatable data.

4.2 Experimental Setup

The generalities of the hardware are explained fully in Chapter 3. This section expands on the specifics of the tactile stimulator in the context of the experiments performed in this work. Two main areas of concern are discussed: 1) the subject's comfort and the associated hardware and 2) the geometry of the indentor.

4.2.1 Subject Comfort

The comfort of the subject demanded attention during the experimental design process. The subject's comfort is important for two reasons. First, the data are more accurate if the subject is comfortable and does not move during the experiments. Second, participation in the scientific experiments should not be harmful to the subject in any way.

The first experimental design consideration from a human factors perspective was the orientation of the hand during the experiments. Data collection sessions lasted between one and three hours; therefore it was important that the subject could relax and be comfortable for an extended period of time. Two options were available for the hand orientation. The subject could either rest his or her hand palm side up, exposing the fingerpad tissue, or the subject could rest his or her hand in the vertical plane. Resting the hand in the vertical plane was found to be the best choice. This was a more natural and comfortable position for subjects, especially over long periods of time. Subjects did not have any excessive twisting in the hand or arm joints in this orientation.

The tactile stimulator is a compact and portable instrument save for the DSP board that is located inside the PC. The portability of mechanical portion of the machine facilitates the comfort of subjects. Once a subject was seated comfortably, the tactile stimulator was moved to the proper position. This configuration avoided awkward or uncomfortable positions that would have otherwise existed due to the variability of the stature of the subjects.

Several other issues concerning the comfort of the subject were addressed in the experimental protocol. First, the subject was seated so that the resting level of the hand was below the heart. Circulation was an important consideration because the finger was constrained and remained motionless for the duration of the experiments. While the fingernail was bonded to a rigid base, several sizes and shapes of foam padding were available to the subject to support his or her wrist and elbow comfortably. As mentioned in Chapter 3, the middle joint of the finger was secured to the steel support platform using a Velcro strap. Ample foam padding was placed between the finger and the platform to

avoid irritation to the knuckle. In a relaxed position, the index finger could interfere with the motion of the tactile stimulator. A padded support strap is located just above the location where the middle finger was secured to the platform. This kept the index finger out the path of the tactile stimulator and allowed the subject to relax the index finger fully during the course of the experiments. As mentioned before, the comfort of the subject was of utmost concern. Once a subject was comfortable, the tactile stimulator was moved to facilitate the position of the subject, not *vice versa*.

Two additional features of the experimental procedure put the subjects at ease. First, the entire procedure was fully explained to the subjects. For example, since the tactile stimulator vibrates, it produces audible noise (random signals and pure tones). An explanation of the these noises before the experiments began prevented subject anxiety. The second feature that put the subjects at ease was incorporated in the software. The computer monitor displayed information about the status of the tests. The tests were automated and the computer displayed the progress of all the experiments, as well as the progress of each test. Downloading the data from each stimulus took approximately five seconds. This period of time was opportune for subjects to make any small movements that were necessary; a display indicated when a subject could move without disturbing the experiments. This type of display also resulted in more accurate and precise data. The duration of each test cycle was 40 seconds. When subjects knew the critical times to hold completely still, and when the subjects knew that an opportunity for movement was approaching, he or she generally tried to adhere to these constraints.

4.2.2 Indentor Geometry

The tactile stimulator allows experiments with displacements that are either normal or tangential to the surface of the fingerpad. A small block at the end of the force sensor permits the indentor to be attached on either of two facets. One facet is parallel to the force sensor mounting surface and the second facet seats the indentor perpendicular to the force sensor mounting surface. The hardware was manually turned to provide the proper direction of displacements and measure the proper corresponding forces.

The indentor design involved two considerations: the shape of the indentor and the dimensions of the indentor. All of the experiments for this research used a flat-ended 1 mm diameter cylindrical punch indentor for experiments in both directions. A cylindrical indentor provided several advantages over other geometries. A flat-bottomed punch gives a simple solution for the elastic case for deformations in the normal and tangential directions (Johnson 1985). Geometries such as cones, spheres, and flat plates introduce contact geometry nonlinearities. Other shapes, such as a rectangular punch, introduce difficulties because of their sharp corners.

The radius of the indentor merited consideration as well. The radius of the indentor must be small in comparison with the radius of the human fingerpad. A small indentor allows the assumption of a semi-infinite half space. This criterion is essential to be able utilize the theoretical results presented in Chapter 2. On the other hand, the indentor cannot be too small. Several problems could occur with an extremely small indentor. First, an extremely small indentor might fall between the ridges of the fingerpad, leading to inconsistent data. Even worse, if the indentor's radius is too small, the indentor might puncture the skin. A small indentor is also difficult to manufacture. A thin probe will buckle or yield even under small forces. The deflections of a thin probe would also corrupt the precision of both the force and the displacement data. As a compromise between all of these considerations, the radius of the punch was chosen to be 0.5 mm. This radius is approximately an order of magnitude smaller than the radius of the human fingerpad; therefore the semi-infinite half space assumption is expected to be valid.

The length of the probe was the final specification for the indentor. The length of the probe should be just long enough to allow the experiments to proceed without the indentor mounting block touching the fingerpad. A short probe reduces deflection of the probe due to the resultant forces of the fingerpad. Taking these two factors into account, the length of the probe protrudes approximately 3 mm from the attachment block.

4.3 Subject Preparation

Several steps were taken to ensure that the data from each subject are consistent in comparison with each trial and also in comparison with the data from other subjects. The subject washed his or her hands in mild soap and room temperature water upon arrival for the experiments. Due to the precision nature of these experiments, varying amounts of oil and dirt particles on the skin could cause inconsistencies in the data. The fingerpad of the middle finger of the right hand was used for all subjects. The middle fingerpad usually lacks the calluses present on the index finger. The right hand is used because this is usually the dominant hand and is used more frequently in gathering tactile information. Also, a consistent location on the fingerpad is important for obtaining repeatable data. For these experiments, the probe location was centered along the width of the fingerpad and at the point on the fingerpad corresponding with one half the length of the attached part of the fingernail. Finally, the subject was required to remain in the test room at least 20 minutes prior to the commencement of the experiments. This allowed time for the fingerpad temperature to equilibrate with the room temperature.

Before the experiments began, the subject's hand was constrained. As mentioned in Chapter 3, the middle joint of the middle finger was secured to a metal platform using Velcro. The index finger was secured in a padded loop above the middle finger. Next, the fingernail of the middle finger was attached with a super glue to the steel platform at a height that placed the probe in line with the targeted location on the fingerpad. This configuration effectively immobilized the fingerpad.

After the subject was comfortable and the finger was constrained, the tactile stimulator was moved to the proper location. The stimulator was commanded to move to the starting position and the probe was aligned normally to the fingerpad at the targeted location. The surface level of the fingerpad was found using a combination of inputs from the subject as well as visual cues. The fingerpad could also be positioned accurately using the micrometer dial located on the steel stage that supported the hand during the experiments. After the finger was positioned, the probe was glued to the fingerpad at the

marked location using a super glue. Only a small amount of glue was used. At the end of the session, the glue was removed using acetone.

One final procedure was necessary to prepare subjects for the experiments. Preconditioning of the fingerpad is essential to obtaining consistent results (Fung 1993). Before the experiments began, a series of five identical preconditioning stimuli were presented to the subject. A random stimulus was used for the preconditioning. These stimuli followed the same form as shown in Figure 4.2. The preindentation depth in the normal direction was 200 μm and no preindentation was used in the tangential direction. The stimuli had a maximum amplitude of 200 μm.

CHAPTER 5
EXPERIMENTAL RESULTS IN THE LINEAR RANGE

Five subjects were used in this study. Table 5.1 gives the ages and genders of the subjects as well as the size measurements of the fingerpad from the distal joint to the fingertip.

Table 5.1: Subject Demographics

Subject	Age	Gender	Length	Width	Thickness
asb	23	F	27.7 mm	14.5 mm	12.2 mm
prb	23	M	29.7 mm	17.8 mm	16.0 mm
ton	24	M	25.6 mm	16.3 mm	13.8 mm
bir	25	M	29.0 mm	16.6 mm	14.1 mm
mnb	27	F	23.0 mm	14.3 mm	11.0 mm

5.1 Confirmation of Linear Range

In order to apply the theory discussed in Chapter 2, it is essential to show that the data collected were indeed in the linear range. Three types of linearity must be assured: contact linearity, geometric linearity, and material linearity.

A consistent contact geometry was assumed for the duration of each experiment. The indentor's radius is small and the entire area of the 0.5 mm radius punch was always in contact with the skin. To further ensure that the condition did not vary during the experiments, the indentor was glued to the fingerpad so that it could not detach from the surface of the skin.

Geometric linearity implies that the displacement gradients are small compared to unity. Material linearity implies that the experiments take place in a linear portion of the stress-strain curve. The experiments conducted in this work measured only displacements and forces. The force-displacement curve is linear if the experiments are in the geometrically linear range and the materially linear range and no contact mechanics nonlinearities are encountered.

As described in Chapter 4, linearity was checked at two frequencies (10 Hz and 100 Hz) using three amplitudes (50 μm, 100 μm, and 150 μm). If the stimuli invoke a linear response, four trends are evident in the force-displacement trajectories. First, the force-displacement curves should be collinear; at the same frequency, the same force should result for a given displacement, regardless of the stimulus amplitude. Second, the force-displacement trajectories should have the same slope for all amplitudes. If the trajectories do not have the same path, the trajectories are most likely to be part of a nonlinear force-displacement curve. Third, the superposition principle should apply; scaling the input by a constant multiplier should give rise to the same scaling of the resulting force. Finally, the force-displacement response is expected to vary with frequency, but both frequencies should show the three linear trends mentioned above.

Figure 5.1 shows that the data collected in this research is in both the geometric linear range and the material linear range. The left hand side of the figure shows the force-displacement trajectories of the stimuli. Each plot shows three traces corresponding to 50 μm, 100 μm, and 150 μm amplitude displacements. The right-hand column of plots shows that the superposition principle applies. The solid lines represent the data in the left-hand column, shifted for viewing purposes so that they are no longer collinear. The dashed lines represent the expected trajectories of the 100 μm and 150 μm amplitude displacement experiments, obtained by scaling the data for the 50 μm amplitude. These predicted results are also shifted from the actual results for viewing purposes.

Linearity Check
Subject: asb

—— Actual Data (Shifted)

—— Actual Data   - - - Data Predicted Using
Superposition (Shifted)

Normal Displacements

Shifted Displacements

Shifted Displacements

Tangential Displacements

Shifted Displacements
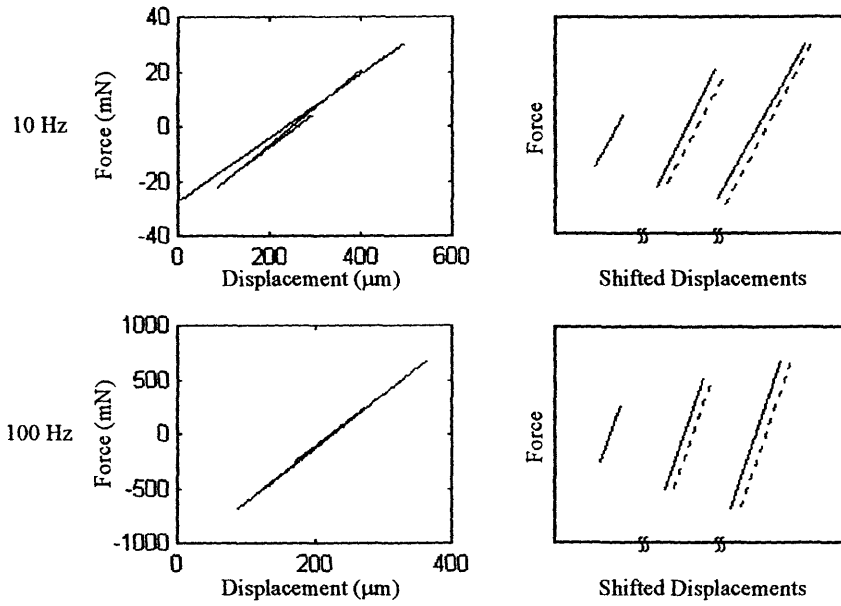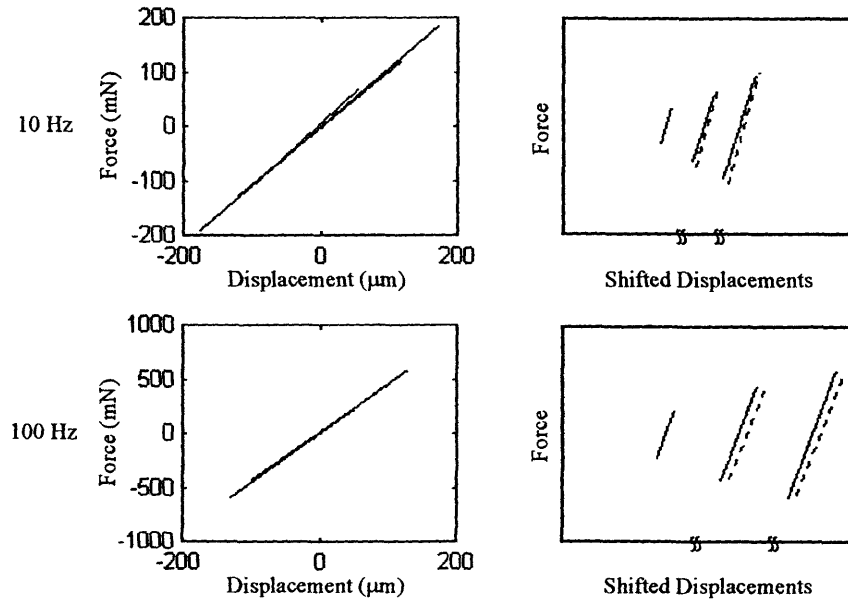
Shifted Displacements

Figure 5.1: Verification of Displacements in the Linear Range

65

The four trends expected for data in the linear range appear in Figure 5.1:

- The force-displacement curves on the left-hand side of Figure 5.1 are collinear.

- The force-displacement trajectories on the left-hand side of Figure 5.1 have approximately the same slope for all three amplitudes at a given frequency.

- The superposition principle applies. The right-hand side of Figure 5.1 shows the actual and expected trajectories. The expected trajectories have approximately the same magnitude and the same slope as the actual data.

- The force-displacement response does vary with frequency, but trajectories at 10 Hz and 100 Hz both show the three linear trends mentioned above.

The observations above hold for displacements in both the normal and tangential directions. The variations in the data were small and can be attributed to noise factors such as small movements by the subject.

The data shown in Figure 5.1 represents only one subject. It is important to perform a linearity check for every subject. The linearity assumption is the basis of the determination of the mechanical properties of the human fingerpad in this study. Since this is a critical assumption, the results of the linearity check for all five subjects appear in Appendix A. The experimental regimes given in Chapter 4 fall within the linear range for all five subjects.

Several observations were made based on the plots shown in Appendix A. Subject bir seems to exhibit a narrower linear range than the other subjects at 10 Hz. The experiment conducted at 10 Hz, 150 μm amplitude shows a slope that is distinct from the slopes of the 10 Hz, 100 μm amplitude experiment and the 10 Hz, 50 μm amplitude experiment. This may be because the 150 μm amplitude experiment invoked a nonlinearity, or it may be to an anomaly in this particular experiment, as is often present with human data.

For all subjects, the experimental data at 100 Hz presented a stronger case for linearity. Slight variations in the slopes of the traces at 10 Hz indicate that the experimental data collected had

more variability at lower frequencies. At 10 Hz, there also seems to be a large difference between the magnitude of the force response in the normal and tangential directions, and also between subjects. This may indicate that the material is actually anisotropic at lower frequencies. It should be noted that the variability in the magnitude of these responses is reduced during the calculation of the material functions.

Also note that the mean force value for most of the experiments is zero. This is because the fingerpad tissue reached a steady state before the stimulus was applied; the steady-state force response of the fingerpad is a very small positive force. The forces are negative for half of the cycle due to the viscoelastic nature of the fingerpad tissue. As the displacements were applied, the fingerpad tissue could not move as quickly as the indentor probe; the tissue relaxed slower than the indentor moved. This resulted in the skin being pulled (negative forces) for half of the cycle. Near the end of the experiments, a steady-state push-pull cycle was established.

One other observation concerns the plots for the linearity check. In the normal direction, for some subjects, the displacement drops below zero. This means that the probe is actually pulling on the skin as opposed to pressing on the tissue. Although this is not intentional, it does not have consequences for the results. The material functions can be measured with the tissue in either tension or compression. This is an artifact of the hardware; the positions can be measured more accurately than they can be controlled. In the tangential direction, the displacements were centered about zero during the data processing procedure. The zero position was visually set before the experiments were run, creating an arbitrary zero position that was adjusted during the data processing. This work is concerned with the amplitude of the responses, not the mean level, so this issue does affect the results.

5.2 Data Processing

Due to the coupling of the inertial response of the force sensor and the force response of the human fingerpad, extensive data processing is necessary to understand the results hidden in the raw data. At most of the experimental frequencies, and especially at higher frequencies, the inertial response of the force sensor is much greater than the response of the fingerpad. At 200 Hz, the magnitude of the inertial response of the force sensor is approximately 20 times larger

67

than the force response of the fingerpad. Accurate data processing is essential to understanding the data collected.

In order to understand the inertial response of the force sensor, all of the experimental paradigms are run on the tactile stimulator with no fingerpad in place (no load condition). Ideally, the force response in all cases is zero; this is not the case with a piezoelectric force sensor. The inertial effects of the system can be modeled by comparing the force response to the commanded displacement in the frequency domain. Several modeling approaches to correct for the inertial response of the force sensor are outlined below.

The system can be modeled using spectral analysis techniques (Inman 1994). Using a random signal as the displacement input yielded a model that showed that the force response is approximately equal to the second time derivative of the displacement multiplied by a constant term (mass), as expected. This model can predict the inertial response with accuracy up to approximately 20 mN.

Figure 5.2 shows the transfer function of the inertial effects. This plot was generated using spectral analysis techniques. If the inertial effects of the force sensor were a mass multiplied by a second derivative, the magnitude would be linear with a slope of 40 dB per decade. Note that the phase is near 0° as opposed to 180° because the displacement is inverted during signal processing to define normal indentations as positive displacements.
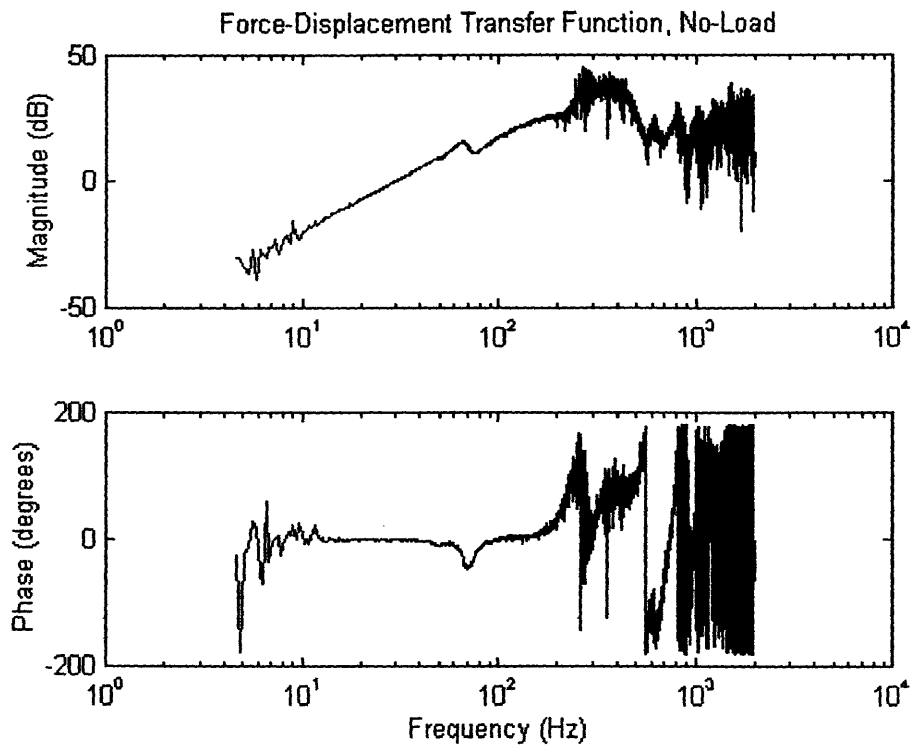
Figure 5.2: Inertial Component of Force Sensor Readings

This method is not precise enough for these experiments. There is too much noise in the approximation at either end of the spectrum. The noise at low frequencies is due to the logarithmic spacing of the analysis points. The noise at high frequencies is due to inconsistent system performance above 300 Hz. A model using a fifth order approximation to a second derivative was also explored. The derivative was too noisy to consider this approach as a viable model.

The alternative models the force sensor's inertial response in the frequency domain using a force-displacement transfer function computed at discrete frequencies. The complex number representing the magnitude and phase of the transfer function at the frequency of interest was recorded and later subtracted from the total response given by the force sensor to give the response of the fingerpad alone. This model is invariant with respect to the amplitude of the displacement and depends only upon frequency. The accuracy of the model is best at low frequencies, predicting the magnitudes within -60 dB at 2 Hz and within -20 dB at 120 Hz.

69

This model is very accurate in the frequency domain, but does not translate well into the time domain due to the finite sampling frequency. For example, at 100 Hz the phase of the modeled transfer function is 74.4°. With a sampling rate of 4000 Hz, the applied phase shift can either be 72° or 81°. At higher frequencies the error can multiply quickly due to the large inertial forces. For this reason, the data can only be modeled accurately in the frequency domain.

In summation, the actual force response of the fingerpad was obtained from the total response of the fingerpad using a simple subtraction of the no load force response from the actual force response. This simplifying assumption can be further refined in the future if more accurate results are desired.

Data processing began as the data were first collected from the force and position sensors. To reduce the size of the data files, data acquisition occurred only during the 10 second stimulus. When the force and displacement data arrived at the A/D card on the computer, the data had already passed through the analog filters described in Chapter 3. As the data were acquired, they were passed through a Hanning window to reduce aliasing of startup and ending transients. The data were sent to the PC in four blocks for each variable. More blocks of data take more time while fewer blocks of data are difficult for the PC/DSP board interface to handle. The PC wrote the data to binary Matlab files.

After the data were written as a binary file, all subsequent processing occurred in the Matlab environment. First, the data were transformed from voltages to mN and μm using the calibration factors and biases listed in Chapter 3. Next, the displacements and forces were passed through bandpass filters that centered around the stimulation frequency. The filtered forces and displacements were corrected for the effects due to filtering. The bandpass filters erased the mean level of forces and displacements; the mean levels were added back into the filtered forces and displacements by adding a value equal to the mean of the raw data.

After the data were filtered, the transfer function of the filtered force to the filtered displacement was calculated at the frequency of the experiment. The transfer function represents the average relationship between the force and displacement over a time period corresponding to seconds 5

through 8.75 of the data collected (that is, data points numbered 20,000 to 35,000). This allowed the response to reach steady state, averaged out any noise that might be present in the data, and avoided characterizing the startup effects of the filter. This transfer function represents the coupled force response of the fingerpad and the inertial effects of the force sensor. The complex number representing the inertial transfer function at the experimental frequency was subtracted from the complex number representing the overall transfer function to give the force-displacement transfer function of the fingerpad. The inertial transfer function can be subtracted from the overall transfer function because the inertial transfer function varies only with the frequency, not the amplitude. Appendix B gives the specifics of the data processing procedure.

Two assumptions are present in the data processing procedures described above: 1) the deformations of the force sensor and the stimulator arm are small and 2) the forces exerted by the fingerpad do not significantly affect the measured, no load inertial characteristics.

As mentioned before, it does not make sense to view most of the data in the time domain; however, at 2 Hz, the inertial effects of the force sensor are negligible. Figure 5.3 shows the data throughout the processing procedure for a stimulus in the normal direction with 200 µm preindentation and a 150 µm amplitude sine wave at 2 Hz.
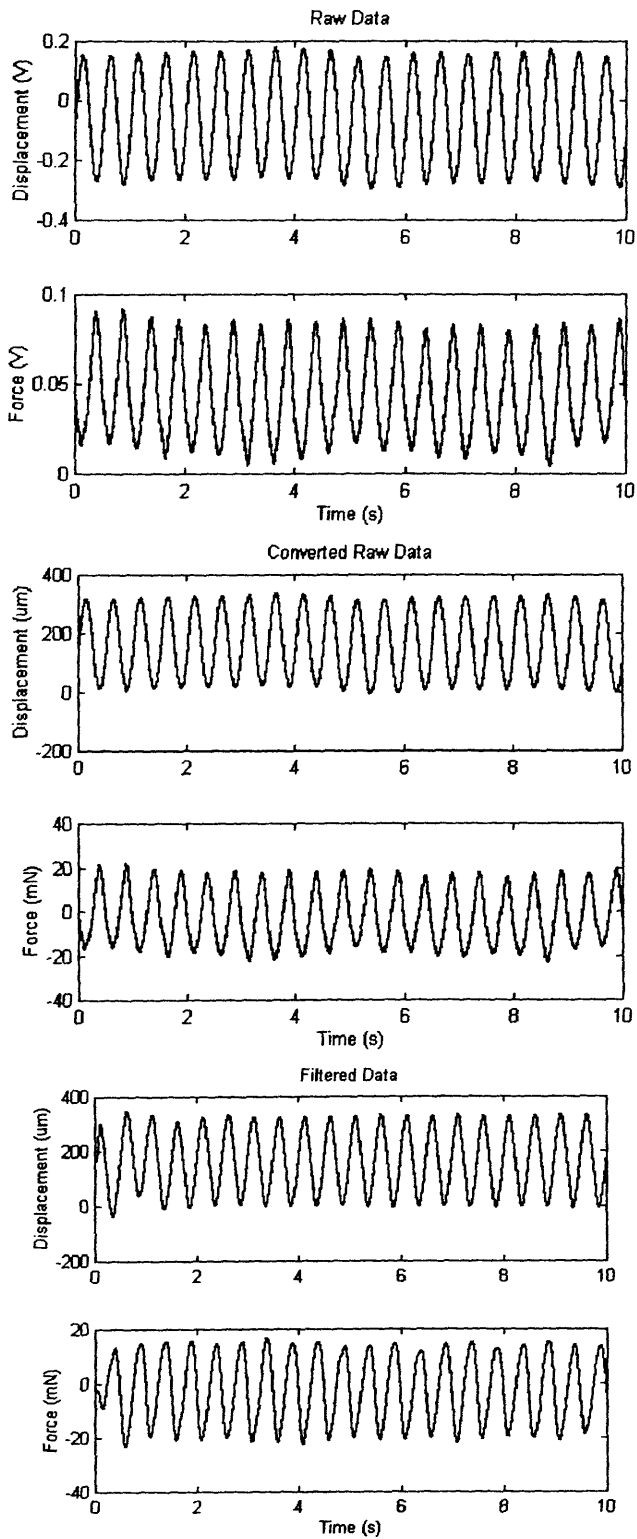
Figure 5.3: Experimental Data for Subject bir in the Normal
Direction

After the data were processed, all of the discrete transfer function values were plotted to obtain an overall transfer function in both the normal and tangential directions. All data points collected for one subject and the corresponding transfer functions are shown in Figure 5.4.

Figure 5.4: Normal and Tangential Transfer Functions for subject bir, all data points

The data shown in Figure 5.4 is repeatable and consistent. The overall normal and tangential transfer functions are an average of the data collected for each subject. Figure 5.5 shows the average of the data collected for all five subjects.

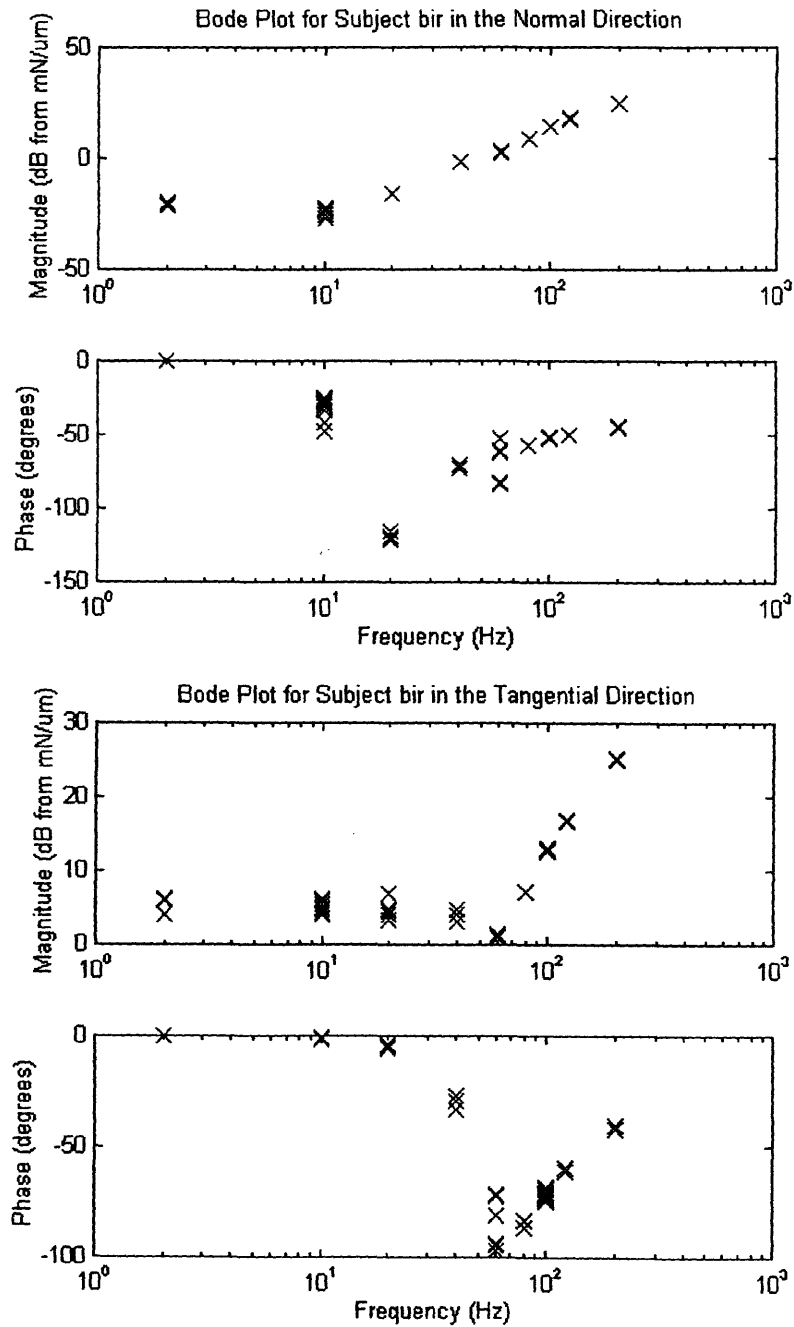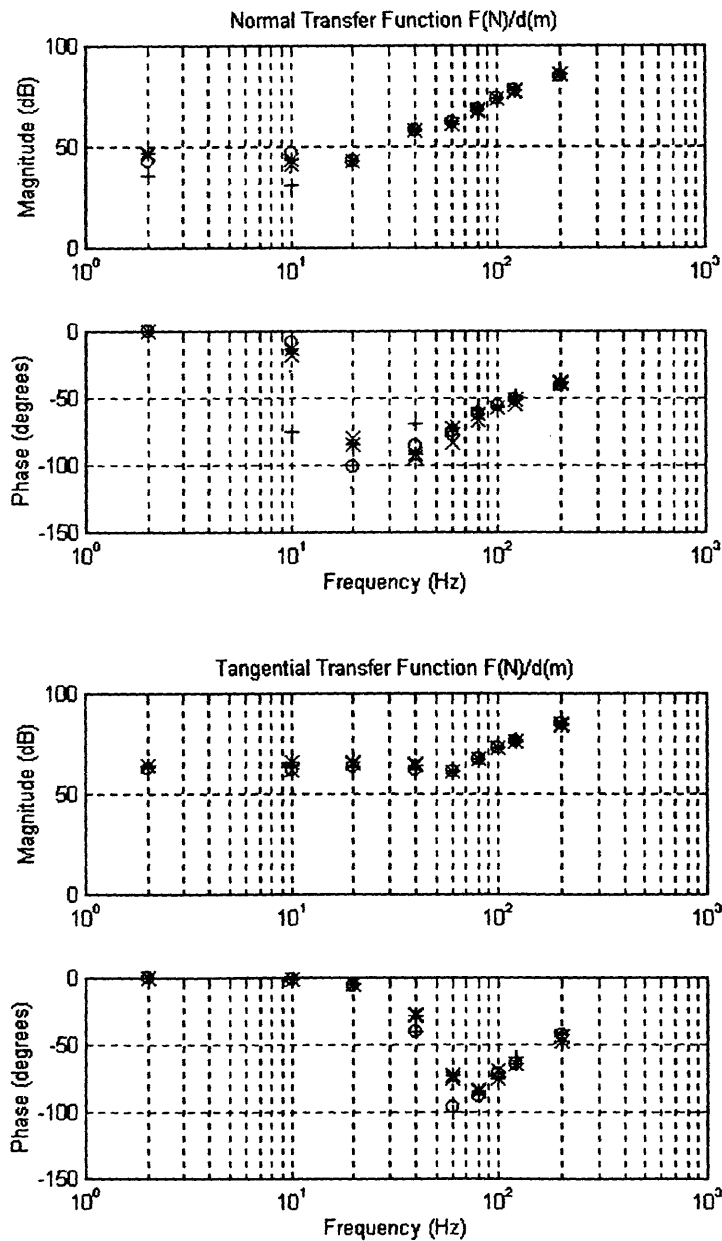Figure 5.5: Normal and Tangential Bode Plots for all subjects

5.3 Discussion of Results

Figure 5.4 and Figure 5.5 show the remarkable consistency of the data collected for one subject and the consistency between the five subjects. Most of the data collected previously (Gulati and Srinivasan 1995, 1997, Pawluk and Howe 1996a,b) show large variations between subjects. Remaining within the linear range may have contributed to more consistent data. Avoiding contact mechanics that cannot be fully predicted throughout the data collection process might have also aided in reducing variability within and between subjects.

Figure 5.5 shows results that are consistent with the research of Pawluk and Howe (1996a,b) and Serina *et al.* (1997). Converting Pawluk's and Howe's step function stiffness values to dB (N/m) resulted in stiffnesses between -20 dB and 75 dB. Serina *et al.* plotted the frequency response of the human fingerpad for a 1 N force over the range of 0 Hz to 3 Hz. Her stiffness values for a 45° indentation were between 60 dB and 75 dB. The data presented in this dissertation are consistent with stiffness values found by previous researchers. The validity of this comparison is somewhat limited because the previous data were collected using large, flat indentors that induced contact mechanics nonlinearites.

The plots in Figure 5.5 also have similar shapes, shifted in frequency and magnitude. It is reasonable to expect that the tissue behaves similarly with respect to frequency under normal and tangential loading. The tissue would also be expected to be stiffer at high frequencies for displacements in either direction.

The Bode plots in Figure 5.5 provide a solution to the specific problem at hand. Developing a model by converting these transfer functions back into the time domain results in the solution of a 0.5 mm radius punch indenting the fingerpad in the linear range for any time history of displacements in either the normal or tangential directions. Chapter 6 addresses the general solution of the viscoelastic material properties of the human fingerpad.

CHAPTER 6
LINEAR VISCOELASTIC MECHANICAL PROPERTIES

The reasons why the tissue can be modeled as a linear viscoelastic material, presented in Chapter 2, are reiterated here (De and Srinivasan 1998):

- The force response is strain rate dependent, evidenced by a dependence on ramp velocity for ramp-and-hold experiments.

- The force response shows stress relaxation; the force response decreases from a peak force value to a steady state value.

- Energy dissipation is observed in the form of hysteresis.

As explained in Chapter 2, the transfer functions derived from the normal and tangential experiments can be used with two linearly independent equations to derive the viscoelastic mechanical properties of a material. Any two material parameters fully describe an elastic material. Similarly, any two of frequency dependent linear viscoelastic material functions can fully describe a viscoelastic material. Two linearly independent frequency dependent material functions are shown for all five subjects in Figure 6.1.
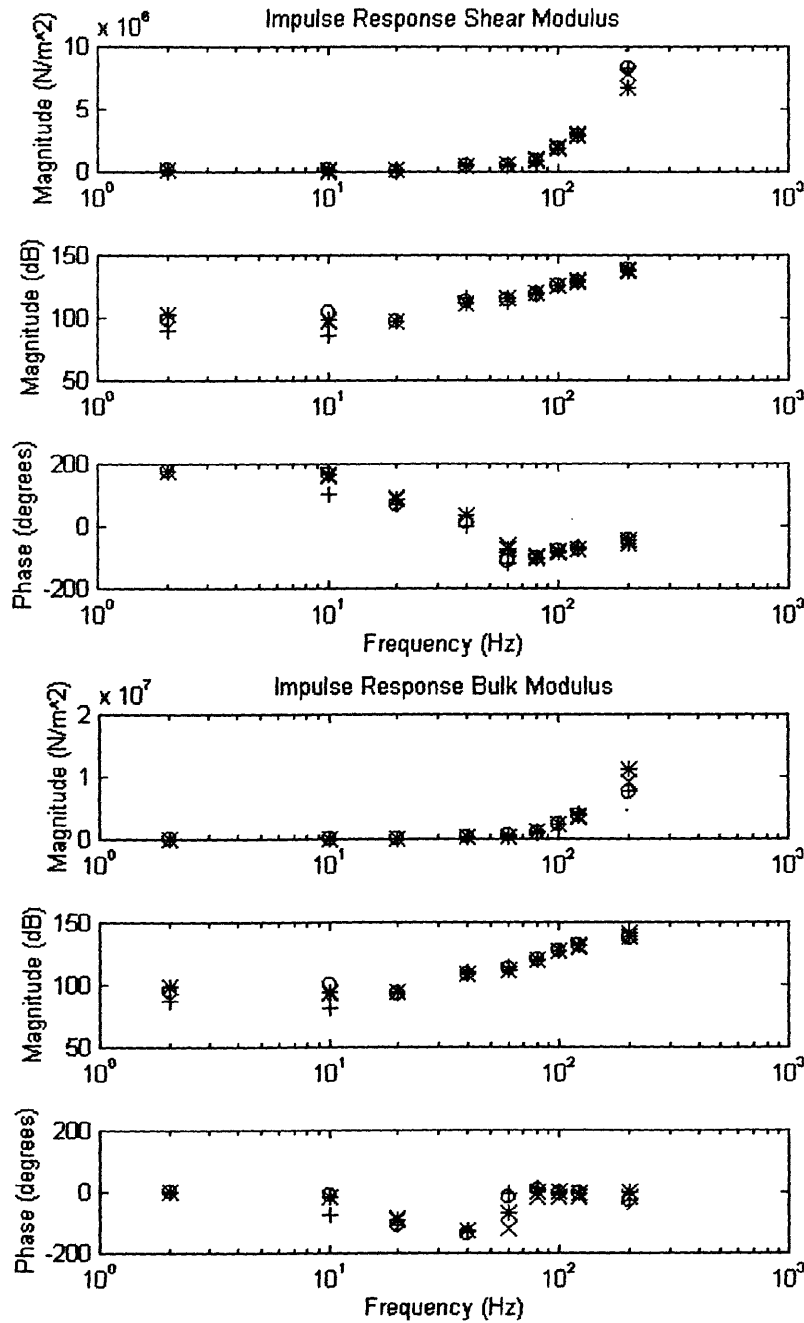
Figure 6.1: Linear Viscoelastic Mechanical Properties of the Human Fingerpad

Three plots represent each property. The top plot represents the magnitude of the value of the mechanical function in Pascals. The middle plot is again a magnitude plot, but uses dB as the units to facilitate viewing the mechanical properties at low frequencies. The bottom plot represents the phase associated with each complex mechanical property. The phase plots are consistent with the values expected from a minimum phase system.

The values shown in Figure 6.1 are given in Table 6.1. The values represent the mean value across all subjects.

Table 6.1: Linear Viscoelastic Mechanical Properties of the Human Fingerpad

Frequency (Hz)	Impulse Response Shear Modulus	Impulse Response Bulk Modulus
2	90 kPa	55 kPa
10	74 kPa	45 kPa
20	70 kPa	47 kPa
40	454 kPa	281 kPa
60	478 kPa	363 kPa
80	908 kPa	986 kPa
100	1.85 MPa	2.25 MPa
120	2.93 MPa	3.79 MPa
200	8.09 MPa	7.56 MPa

The shear modulus is a measure of the ratio of shear stresses to the shear strains in the tangential direction. The shear modulus is expected to monotonically increase for a linear viscoelastic material. This is the response expected of a viscoelastic material as defined by Tschoegl (1989). This trend is shown in the experimental results. The shear modulus falls within a range of 90 kPa to 8 MPa.

The bulk modulus is a measure of the overall response of a tissue to a deformation. Specifically, the bulk modulus is a measure of relationship between volumetric (or bulk) stress and volumetric strain. The bulk modulus is expected to increase monotonically as well. The bulk modulus falls within a range of 55 kPa to 8 MPa.

One physical interpretation of the linear viscoelastic impulse response material properties can be made. Using the final value theorem of the Laplace transform, the material functions at a frequency of zero represent the steady state values of the properties in the time domain, also the elastic parameters. The assertions that we can make are that the elastic shear modulus is on the order of 90 kPa and the elastic bulk modulus is on the order of 55 kPa. These are the impulse response material functions at 2 Hz.

One interesting observation is that the mechanical properties exhibit the most variability at high frequencies. Considering the inertial corrections for the forces, this is the expected outcome. One other factor that could play a role in this variability is the mass of the fingerpad. The calculations for the material functions assume that the mass of the fingerpad is negligible. Several researchers have shown that the mass of the fingerpad plays a role in the viscoelastic model when the frequency is higher than about 200 Hz (Pawluk and Howe 1996a,b, Kárason *et al.* 1998).

One final observation is the ratio of the bulk modulus to the rigidity modulus. If this ratio is large, the material is considered incompressible. These results show that this ratio is only on the order of 0.5 at 2 Hz. This ratio implies that the material is indeed compressible. From previous studies, this ratio was expected to be much larger; therefore this assertion needs to be verified independently.

CHAPTER 7

SUMMARY

7.1 Tactile Stimulator

The tactile stimulator is a versatile device that can provide a variety of stimuli to any material and measure the displacement and force responses of the material. The stimuli can be varied with time or with indentor shape and the device is currently configured to allow normal or tangential displacement-controlled stimuli. The tactile stimulator measures forces with a precision of less than 1 mN and displacements with a precision of less than 1 μm. The software developed for the tactile stimulator allows an automated set of tests or individual tests to be performed. The programs can easily be modified to introduce a new set of stimuli. This hardware was designed from a haptics viewpoint, but could be used with any material to determine the mechanical properties. The device could also be used for perceptual experiments within the field of haptics.

7.2 Linear Viscoelastic Mechanical Properties of the Human Fingerpad

The solution to the linear elastic problem of a cylindrical punch indenting a semi-infinite half-space can be transformed to a linear viscoelastic solution by means of the correspondence principle. Two mechanical properties of a material can completely

describe any force-displacement or stress-strain relationship within the material. To determine the mechanical properties of the human fingerpad, two linearly independent experiments were performed to solve for the dynamic, viscoelastic mechanical properties of the human fingerpad. A variety of normal and tangential vibrational stimuli were applied to the fingerpad to obtain the transfer functions of the force-displacement relationship in both directions. All of the experiments were conducted in the linear range of the tissue.

The impulse response bulk modulus and the impulse response shear modulus are defined in this thesis as a function of frequency. These properties can be transformed back to the time domain to completely describe the three-dimensional linear viscoelastic behavior of the human fingerpad tissue in the linear range. The data obtained in this research is consistent within a subject and across subjects. Results suggest that the fingerpad tissue may be compressible.

7.3 Future Work

7.3.1 The Tactile Stimulator

The tactile stimulator can be used for many applications in the area of haptics. A further analysis of the dynamics of the machine could enhance the performance of the device. First, a model of system dynamics would allow the user to implement an optimal controller. The controller in this work was developed only by using a modified tuning method. During characterization of the ramp response of the tactile stimulator, the pattern of overshoots indicates that the system is nonlinear. Adaptive control techniques would be particularly useful for optimizing the performance of this system. A model of the dynamics of the system also allows force-controlled algorithms to be implemented.

The tactile stimulator also needs a more precise model of the force sensor dynamics. The accelerations measured by the force sensor were generally greater than the force response of the human fingerpad. In order to be confident of the force sensor's performance for

stimuli other than those used in this research, a more comprehensive model of the force sensor behavior is necessary.0

Further validation of the performance of the machine would also be useful. Performing the same tests described in this dissertation on a piece of material with known parameters, such as a spring or a piece of rubber, would allow the machine and data processing procedures to be verified and fine-tuned.

7.3.2 Characterization of the Nonlinear Range of the Fingerpad Tissue

A natural extension of this work is to continue modeling the viscoelastic material properties of the human fingerpad at deeper indentations that are in the nonlinear range of the material. The methods presented in this work are not sufficient to characterize geometric, material, or contact nonlinearities.

7.3.3 Characterization of the Mechanoreceptors

Finally, the linear viscoelastic mechanical properties of the human fingerpad found in this research contribute to the understanding of the human tactile system. The mechanical properties of the fingerpad allow hapticians to develop models for the stress-strain fields within the fingerpad tissue for any geometry stimulus with any time history. These stress-strain fields are the root of understanding the neural responses that are sent to the brain when we touch an object. Utilizing the mechanical properties revealed in this research will eventually allow better virtual environments, more useful prosthetics, and enhance industrial capabilities.

APPENDIX A

LINEARITY CHECK

This appendix contains the linearity analysis for each subject. The plots clearly show that the experimental data were collected in the linear range.

The plots in the left-hand column each contain three curves that represent force-displacement trajectories. All of the curves are at approximately the same depth of indentation in the normal direction and at the neutral position in the tangential direction. Each curve within a single plot represents a different amplitude sinusoid (approximately 50 μm, 100 μm, and 150 μm amplitudes).

The plots in the right-hand column demonstrate that superposition applies. In these plots, the abscissa is shifted for each curve so that the lines are not collinear. The solid lines represent the actual data shown in the corresponding plot on the left hand side. The dashed lines represent the data prediction assuming superposition of the appropriate number of 50 μm amplitude curves.

See Section 5.1 for a complete analysis of these curves.

Linearity Check

Subject: asb

—— Actual Data

—— Actual Data (Shifted)
- - - Data Predicted Using
Superposition (Shifted)

Normal Displacements
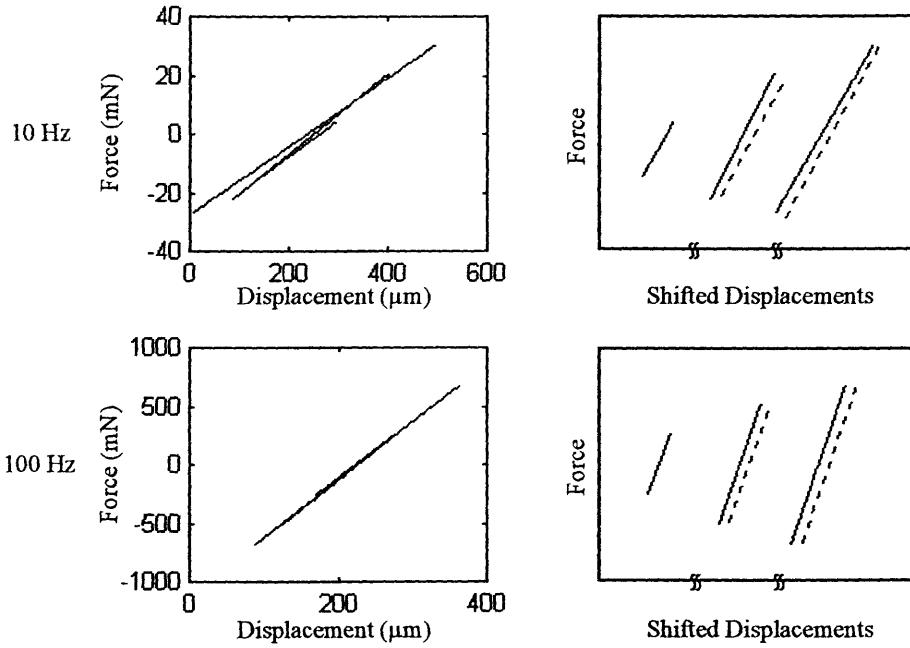
Tangential Displacements

Linearity Check
Subject: prb

———Actual Data

——— Actual Data (Shifted)

– – – Data Predicted Using
Superposition (Shifted)

Normal Displacements

Tangential Displacements
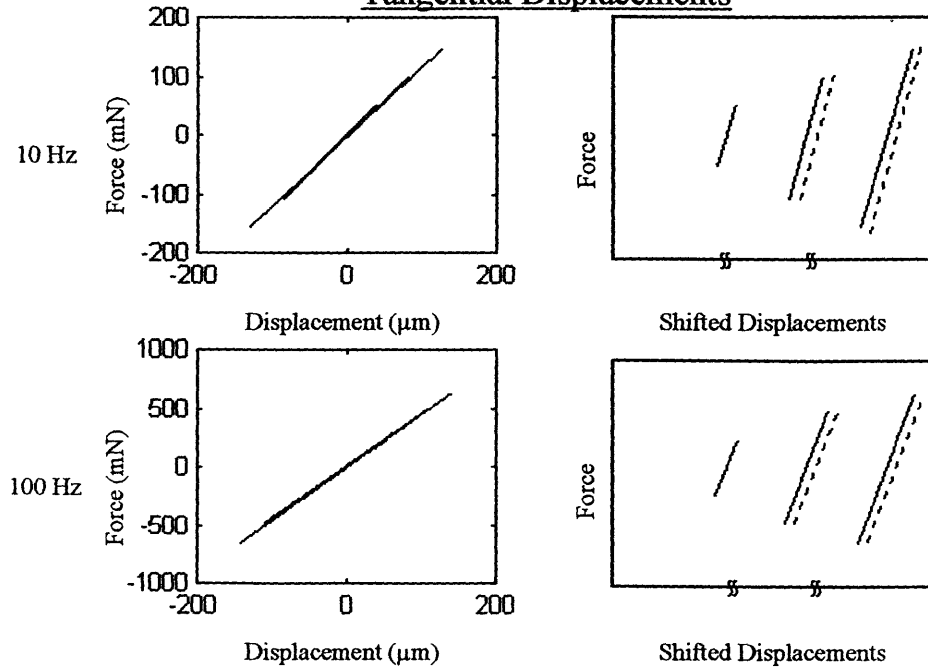
Linearity Check
Subject: ton

— Actual Data

—— Actual Data (Shifted)
- - - Data Predicted Using
Superposition (Shifted)

Normal Displacements

10 Hz

100 Hz

Shifted Displacements

Shifted Displacements

Tangential Displacements

10 Hz

100 Hz

Shifted Displacements
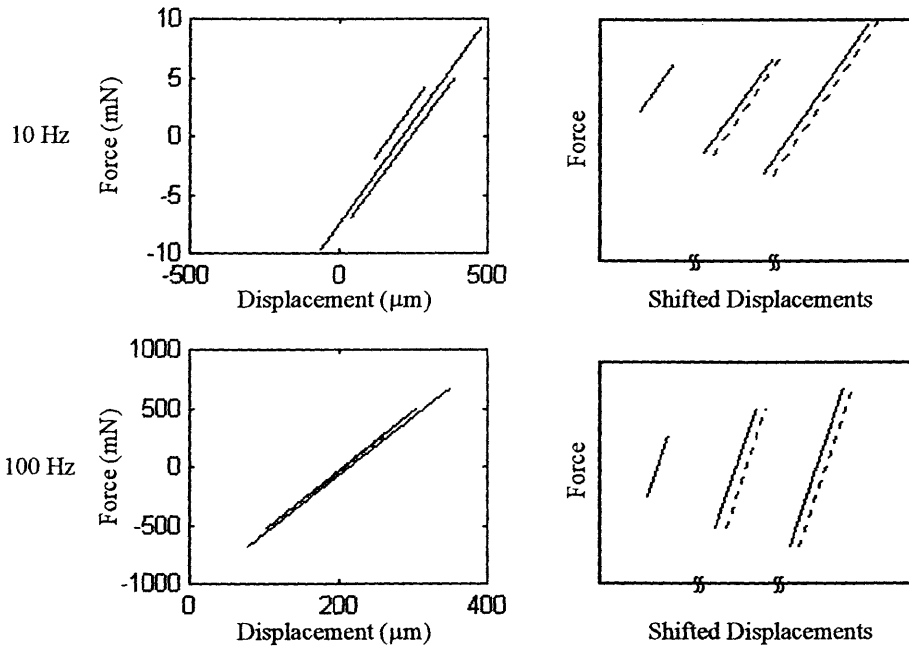
Shifted Displacements
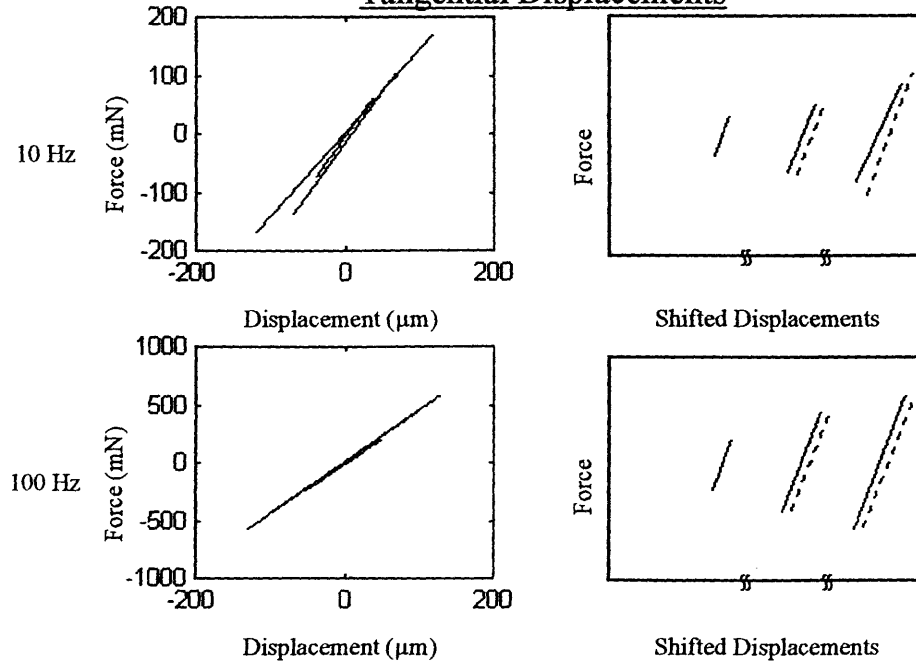
Linearity Check
Subject: bir

——Actual Data

—— Actual Data (Shifted)
- - - Data Predicted Using
Superposition (Shifted)

Normal Displacements

10 Hz

Shifted Displacements

100 Hz

Shifted Displacements

Tangential Displacements

10 Hz

Shifted Displacements

100 Hz

Shifted Displacements

89
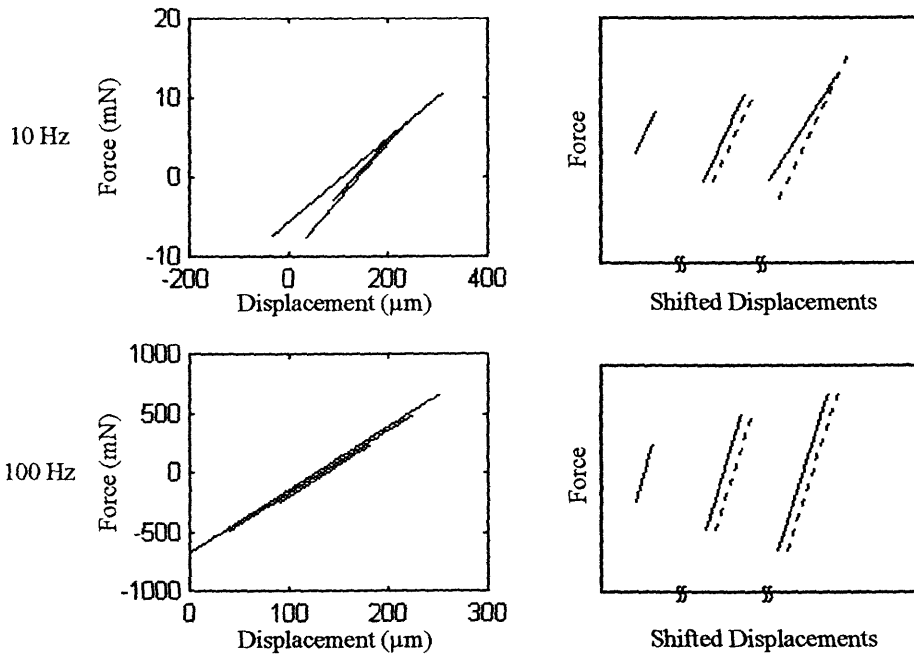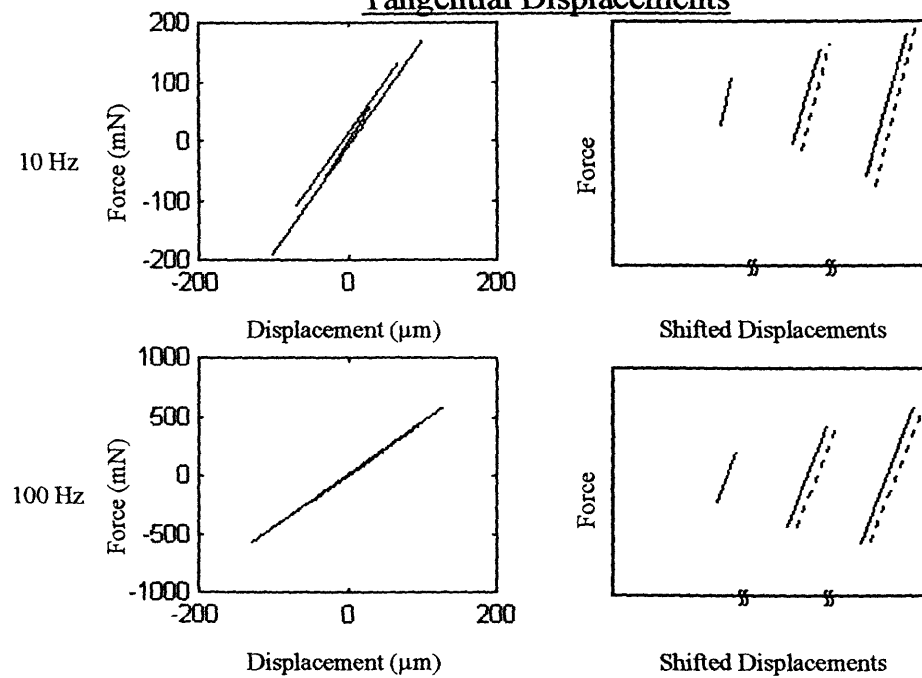
Linearity Check
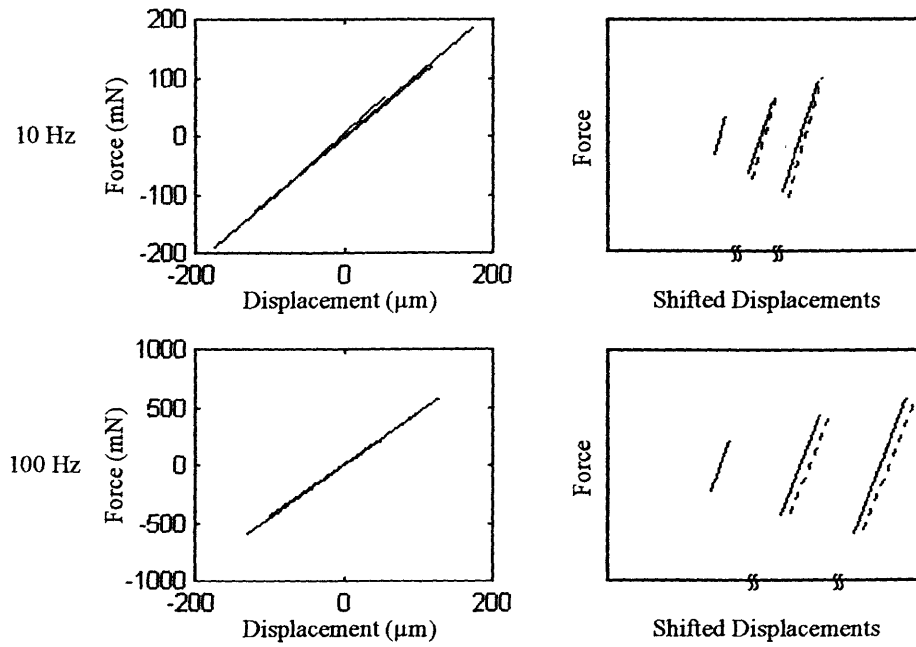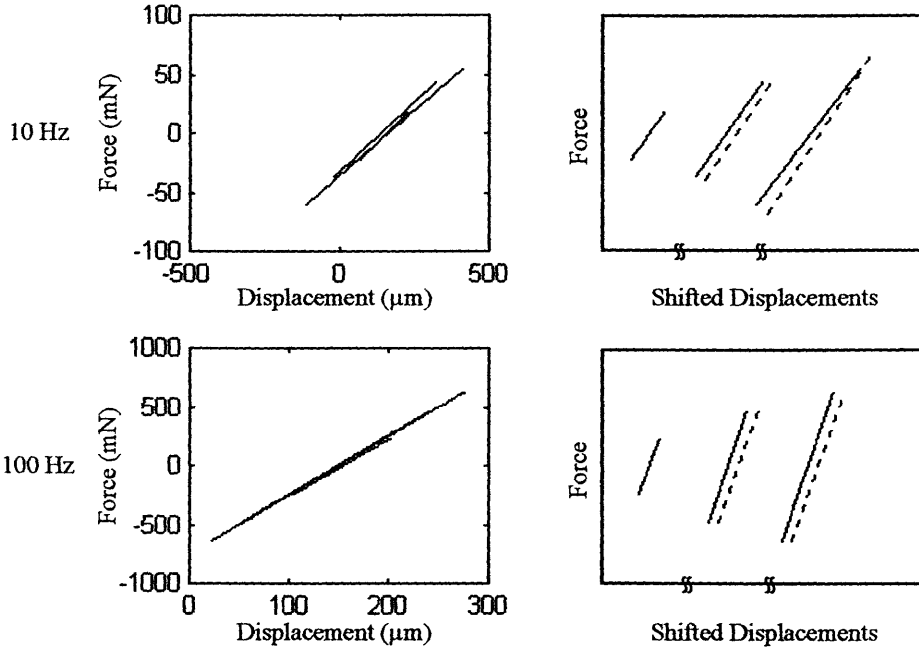## Subject: mnb

—— Actual Data

—— Actual Data (Shifted)
- - - Data Predicted Using
      Superposition (Shifted)

Normal Displacements

10 Hz

100 Hz

Shifted Displacements

Shifted Displacements

Tangential Displacements

10 Hz

100 Hz

Shifted Displacements

Shifted Displacements

90
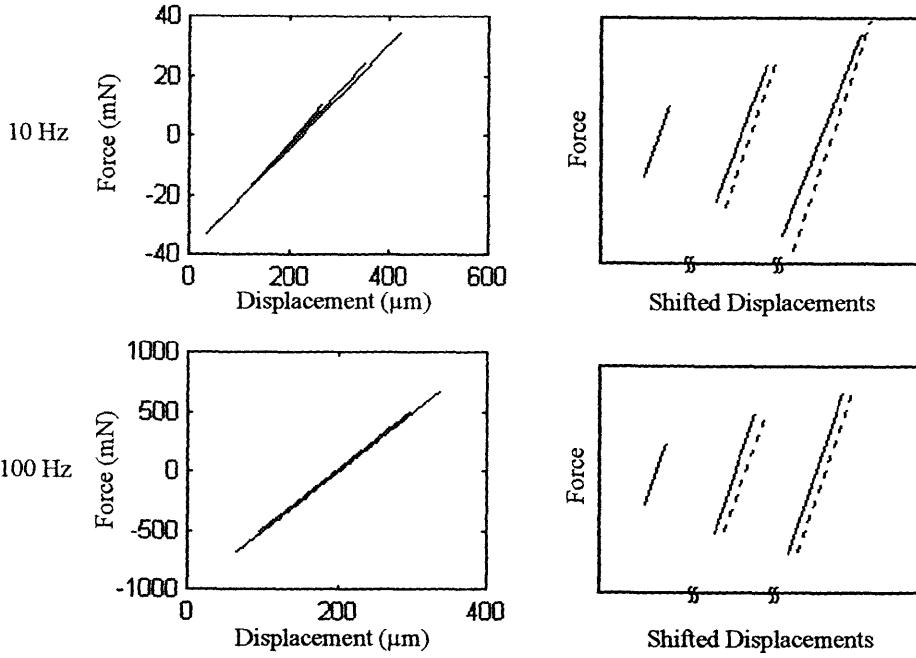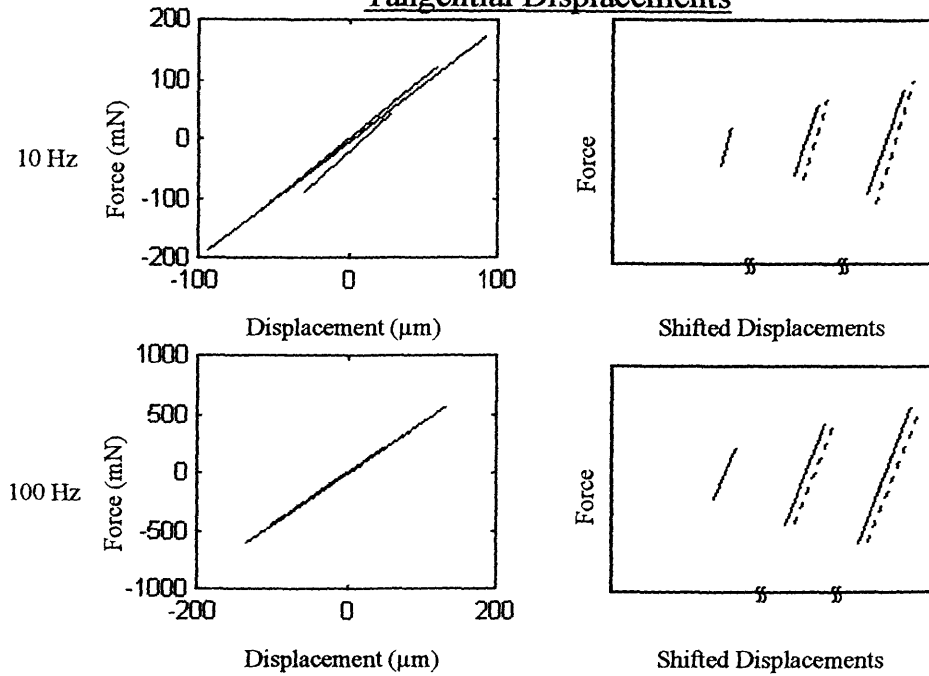
APPENDIX B

DETAILED EXPLANATION OF THE DATA PROCESSING

This appendix describes the data processing procedure in detail in both graphical and tabular form.

```
┌─────────────────────┐          ┌─────────────────────┐
│ Calibration Correction/│       │ Calibration Correction/│
│   Conversion to μm   │          │   Conversion to μN   │
└─────────────────────┘          └─────────────────────┘
           │                                │
           ▼                                ▼
      ┌─────────┐                      ┌─────────┐
      │ Filter I│                      │ Filter II│
      └─────────┘                      └─────────┘
           │                                │
           ▼                                ▼
      ┌─────────┐                      ┌─────────┐
      │ Filter II│                     │ Filter II│
      └─────────┘                      └─────────┘
           │                                │
           ▼                                ▼
      ┌─────────┐                      ┌─────────┐
      │ Filter II│                     │ Filter II│
      └─────────┘                      └─────────┘
           │                                │
           ▼                                ▼
      ┌─────────┐                      ┌─────────┐
      │  Filter │                      │  Filter │
      │Correction│                     │Correction│
      └─────────┘                      └─────────┘
            ╲                          ╱
             ╲                        ╱
          ┌─────────────────────────────┐
          │  Overall Transfer Function  │
          └─────────────────────────────┘
                        │
                        ▼
       ┌──────────────────────────────────┐
       │ Subtract Inertial Transfer Function│
       └──────────────────────────────────┘
                        │
                        ▼
        ┌─────────────────────────────┐
        │  Fingerpad Transfer Function │
        └─────────────────────────────┘
```
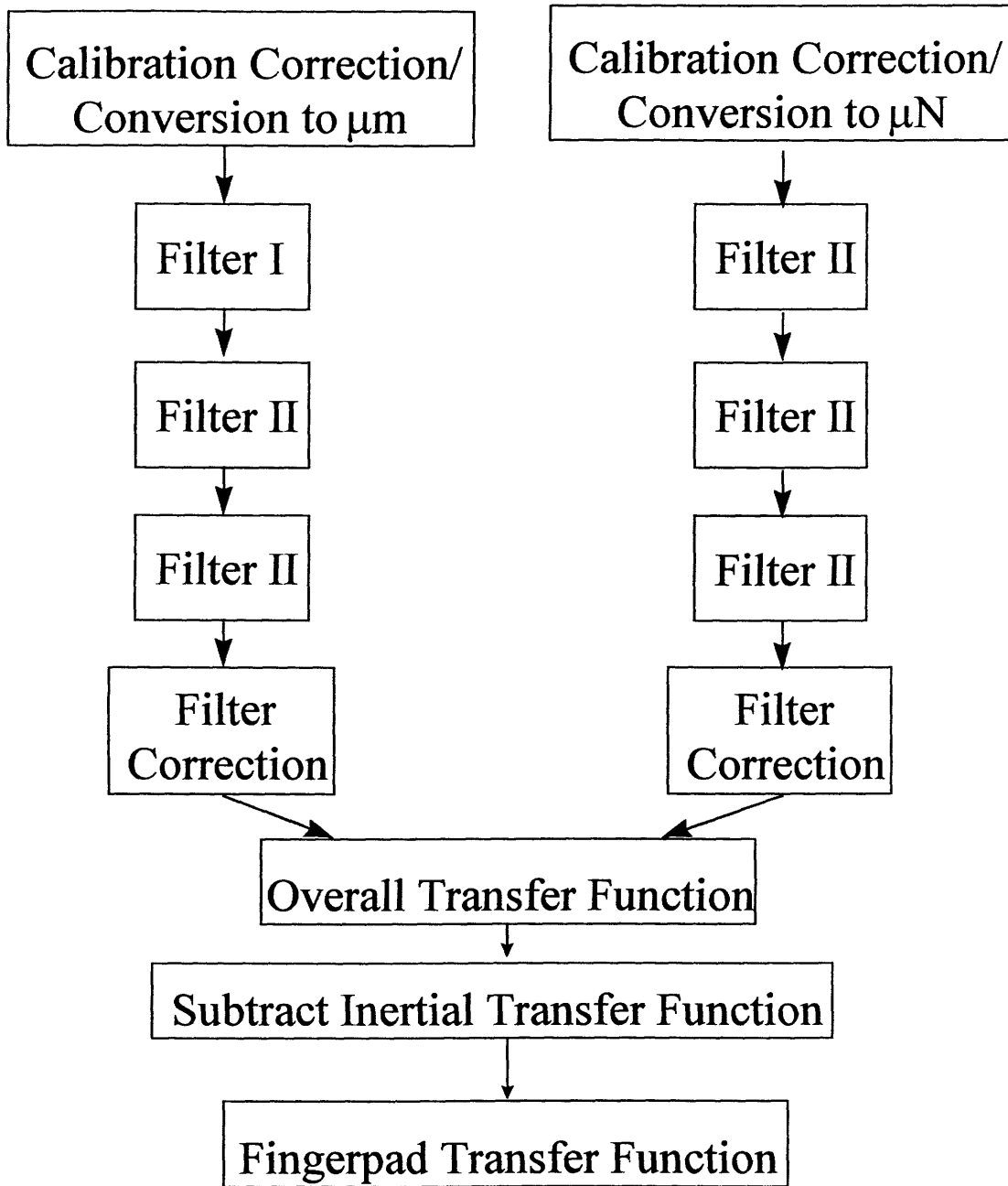
Parameters for all the blocks in the figure above follow in tabular form.

Calibration Conversions

	Conversion	Bias
Displacement	717 μm/V	-8 μm
Force	512.44235 mN/V	24.9 mN

Parameters of Filter I: A 2nd Order Butterworth Bandpass Filter
Low Frequency Cutoff: 0.5 Hz
High Frequency Cutoff: 300 Hz

Parameters of Filter II: A 2nd Order Butterworth Bandpass Filter

Frequency (Hz)	Lowpass Cutoff (Hz)	Highpass Cutoff (Hz)
2	0.5	10
10	5	20
20	10	40
40	20	60
60	40	80
80	60	100
100	80	120
120	100	140
200	180	220

Filter Correction Factors

Frequency (Hz)	Displacement Correction	Force Correction
2	1.0001∠-28.85°	1.0008∠3.64°
10	1.0000∠-1.41°	1.0302∠43.34°
20	1.0000∠3.26°	1.0309∠43.26°
40	1.0038∠50.94°	1.1003∠121.36°
60	1.0014∠42.62°	1.1482∠108.30°
80	1.0024∠41.45°	1.1872∠102.68°
100	1.0055∠43.18°	1.2167∠99.58°
120	1.0115∠46.44°	1.2399∠97.63°
200	1.0897∠66.52°	1.2952∠93.93°

Inertial Correction Factors Including the Angle from the Filter Correction Factors

Frequency (Hz)	Correction Factor
2	$0.0011\angle 12.6721°$
10	$0.0500\angle 43.2349°$
20	$0.2082\angle 42.8610°$
40	$0.9344\angle 57.2206°$
60	$2.0000\angle 36.0°$
80	$2.4844\angle 65.9316°$
100	$4.3266\angle 74.4031°$
120	$6.1394\angle 78.0°$
200	$12.1099\angle 102.0°$

Beer, Ferdinand P., and E. Russell Johnston, Jr. 1992. *Statics and Mechanics of Materials*. New York: McGraw-Hill, Inc.

Bolanowski, S. J., Jr., G. A. Gescheider, R. T. Verrillo, and C. M. Checkosky. 1988. "Four Channels Mediate the Mechanical Aspects of Touch." *The Journal of the Acoustical Society of America*. 84: 1680-1694.

Christensen, R. M. 1971. *Theory of Viscoelasticity: An Introduction*. New York: Academic Press, Inc.

Cook, Nathan H., and Ernest Rabinowics. 1963. *Physical Measurement and Analysis*. Reading: Addison Wesley.

Dandekar, K, and M. A. Srinivasan. 1995. "A 3 Dimensional Finite Element Model of the Monkey Fingertip for Predicting Responses of Slowly Adapting Mechanoreceptors." *Bioengineering Conference Summer Annual Meeting of the ASME*.

De, Suvranu. 1998. Unpublished observations.

De, Suvranu, and Mandayam A. Srinivasan. 1998. "A Finite element Model of the Human Fingerpad Incorporating Viscoelasticity." Manuscript in preparation.

DeVor, Richard E., Tsong-how Chang, and John W. Sutherland. 1992. *Statistical Quality Design and Control: Contemporary Concepts and Methods*. New York: Macmillan Publishing Company.

Doebelin, Ernest O. 1980. *System Modeling and Response: Theoretical and Experimental Approaches*. New York: Wiley.

Doebelin, Ernest O. 1983. *Measurement Systems: Applications and Design*. 3rd ed. New York: McGraw Hill.

Ewins, D. J. 1984. *Modal Testing: Theory and Practice*. New York: Research Studies Press.

Figliola, Richard S., and Donald E. Beasley. 1991. *Theory and Design for Mechanical Measurements*. New York: John Wiley.

Finlay, B. 1970. "Dynamic Mechanical Testing of Human Skin *In Vivo*." *Journal of Biomechanics*. 3: 557-568.

Franklin, Gene F., J. David Powell, and Michael L. Workman. 1990. *Digital Control of Dynamic Systems*. 2nd ed. Reading: Addison-Wesley Publishing Company.

Fung, Y. C. 1993. *Biomechanics: Mechanical Properties of Living Tissues*, 2nd ed. New York: Springer-Verlag.

Gautschi, G. H. 1978. *Piezoelectric Multicomponent Force Transducers and Measurement Systems*. Amhearst: Kistler Instrument Corporation.

Gulati, R. J. and M. A. Srinivasan. 1995. "Human Fingerpad Under Indentation I: Static and Dynamic Force Response." *Proceedings of the 1995 Bioengineering Conference*. Ed. R. M. Hochmuth, N. A. Langrana, and M. S. Hefzy. 29: 261-262.

Gulati, Rogeve J., and Mandayam A. Srinivasan. 1997. *Determination of Mechanical Properties of the Human Fingerpad*, In Vivo, *Using a Tactile Stimulator*. Massachusetts Institute of Technology Research Laboratory of Electronics Technical Report 605.

Hajian, Aram Z., and Robert D. Howe. 1994. "Identification of the Mechanical Impedance of Human Fingers." *Proceedings of the ASME Winter Annual Meeting, Dynamic Systems and Control, Volume I*. 55: 319-327.

Horowitz, Paul, and Winfield Hill. 1989. *The Art of Electronics*. New York: Cambridge University Press.

Inman, Daniel J. 1994. "Chapter 7: Vibration Testing and Experimental Modal Analysis." *Engineering Vibration*. Englewood Cliffs: Prentice Hall.

Johansson, R. S., U. Landström, and R. Lundström. 1982. "Responses of Mechanoreceptive Afferent Units in the Glabrous Skin of the Human Hand to Sinusoidal Skin Displacements." *Brain Research*. 244:17-25.

Johnson, K. L. 1985. *Contact Mechanics*. Cambridge: Cambridge University Press.

Juvinall, Robert C., and Kurt M. Marshek. 1991. *Fundamentals of Machine Component Design*. 2nd ed. New York: John Wiley and Sons.

Kandel, Eric R., and Thomas M. Jessell. 1991. "Chapter 26: Touch." *Principles of Neural Science*. 3rd ed. Norwalk: Appleton and Lange.

Kárason, S. P., A. Annaswamy, and M. A. Srinivasan. 1998. *Identification and Control of Haptic Systems: A Computational Theory*. Massachusetts Institute of Technology Research Laboratory of Electronics Technical Report 621.

Karu, Zoher Z. 1995. *Signals and Systems Made Ridiculously Simple*. Cambridge: ZiZi Press.

Kernighan, Brian W., and Dennis M. Ritchie. 1990. *The C Programming Language*. 2nd ed. New Delhi: Prentice Hall of India.

Kiemele, Mark J., and Stephen R. Schmidt. 1993. *Basic Statistics: Tools for Continuous Improvements*. 3rd ed. Colorado Springs: Air Academy Press.

Klafter, Richard D., Thomas A. Chmielewski, and Michael Negin. 1989. *Robotic Engineering: An Integrated Approach*. Englewood Cliffs: Prentice Hall.

Lanir, Y. 1987. "Chapter 11: Skin Mechanics." *Handbook of Bioengineering*. Ed. R. Skalak and S. Chien. New York: McGraw Hill.

Lee, E. H. 1955. "Stress Analysis in Viscoelastic Bodies." *Quarterly Applied Mathematics*. 13:183-190.

Ogata, Katsuhiko. 1990. *Modern Control Engineering*. 2nd ed. Englewood Cliffs: Prentice Hall.

Oppenheim, Alan V, and Alan S. Willsky. With S. Hamad Nawab. 1997. *Signals and Systems*. 2nd ed. Upper Saddle River: Prentice Hall.

Parr, E. A. 1996. *Control Engineering*. Oxford: Butterworth-Heinemann.

Pawluk, Dianne T. B., and Robert D. Howe. 1996a. "Dynamic Contact Mechanics of the Human Fingerpad, Part I: Lumped Response." Submitted to the *Journal of Biomechanical Engineering*.

Pawluk, Dianne T. B., and Robert D. Howe. 1996b. "Dynamic Contact Mechanics of the Human Fingerpad, Part II: Distributed Response." Harvard Robotics Lab Technical Report 96-004.

Phillips, Charles L., and Royce D. Harbor. 1991. *Feedback Control Systems*. 2nd ed. Englewood Cliffs: Prentice Hall.

Phillips, J. R., and K. O. Johnson. 1981. "Tactile Spatial Resolution. III. A Continuum Mechanics Model of Skin Predicting Mechanoreceptor response to Bars, Edges, and Gratings." *Journal of Neurophysiology*. 46: 1204-1225.

Pipkin, A. C. 1972. *Lectures on Viscoelasticity Theory*. New York: Springer-Verlag.

Pubols, Benjamin H., Jr. 1987. "Effect of Mechanical Stimulus Spread across Glabrous Skin of Raccoon and Squirrel Monkey Hand on Tactile Primary Afferent Fiber Discharge." *Somatosensory Research*. 4: 273-308.

Rabinowitz, W. M., A. J. M. Houtsma, N. I. Durlach, and L. A. Delhorne. 1987. "Multidimensional Tactile Displays: Identification of Vibratory Intensity, Frequency, and Contactor Area." *The Journal of the Acoustical Society of America*. 82: 1243-1252.

Sargent, Murray, III, and Richard L. Shoemaker. 1995. *The Personal Computer from the Inside Out: The Programmer's Guide to Low-Level PC Hardware and Software*. 3rd ed. Reading: Addison-Wesley Publishing Company.

Serina, Elaine R., C. D. Mote, Jr., and David Rempel. 1997. "Force Response of the Fingertip Pulp to Repeated Compression—Effects of Loading Rate, Loading Angle and Anthropometry." *Journal of Biomechanics*. 30: 1035-1040.

Siebert, William M. 1986. *Circuits, Signals, and Systems*. Cambridge: MIT Press.

Srinivasan, M. A. 1989. "Surface Deformation of Primate Fingertip Under Line Load." *Journal of Biomechanics*. 22: 343-349.

Srinivasan, M. A., and K. Dandekar. 1996. "An Investigation of the Mechanics of Tactile Sense using Two-Dimensional Models of the Primate Fingertip." *Transactions of the ASME*. 118: 48-55.

Srinivasan, M. A., R. J. Gulati, and K. Dandekar. 1992. "*In Vivo* Compressibility of the Human Fingertip." *Advances in Bioenginieering* 22: 573-576.

Srinivasan, M. A., Rogeve Gulati, and Suvranu De. 1998. "Force Response of the Human Fingerpad to Dynamic Indentations." Submitted to *Journal of Biomechanics*.

Srinivasan, M. A., and R. H. LaMotte. 1995. "Tactual Discrimination of Softness." *Journal of Neurophysiology*. 73: 88-101.

Srinivasan, M. A., and R. H. LaMotte. 1996. "Tactual Discrimination of Softness: Abilities and Mechanisms." *Information Processing in the Somatosensory System*. Ed. O. Franzen, R. Johansson, and L. Terenius. Basel: Birkhauser Verlag AB.

Tan, Hong Zhang. 1996. *Information Transmission with a Multi-Finger Tactual Display*. Ph. D. Dissertation. Department of Electrical Engineering and Computer Science. Massachusetts Institute of Technology.

Tan, Hong Z., and William M. Rabinowitz. 1996. "A New Multi-Finger Tactual Display." *Proceedings of the Fifth Annual Symposium on Haptic Interfaces for Virtual Environment and Teleoperator Systems*. 21-22 Nov. Atlanta: 1996 ASME International Mechanical Engineering Congress and Exposition.

Tschoegl, Nicholas W. 1989. *The Phenomenological Theory of Linear Viscoelastic Behavior*. Berlin: Springer-Verlag.

Vallbo, Å. B. , and R. S. Johansson. 1984. "Properties of Cutaneous Mechanoreceptors in the Human Hand Related to Touch Sensation." *Human Neurobiology*. 3: 3-14.

Von Gierke, Henning E., Hans L. Oestreicher, Ernst K. Franke, Horace O. Parrack, and Wolf W. von Wittern. 1952. "Physics of Vibrations in Living Tissues." *Journal of Applied Physiology*. 4:886-900.

Waite, Mitchell, Stephen Prata, and Donald Martin. 1987. *C Primer Plus*. Revised ed. Indianapolis: Howard W. Sams and Company.

Ziegler, J. B., and N. B. Nichols. 1942. "Optimum Settings for Automatic Controllers." *Transactions of the A.S.M.E.* 64:759-758.